PLOS BIOLOGY

SHORT REPORTS

The evolution of antimicrobial peptide resistance in *Pseudomonas aeruginosa* is severely constrained by random peptide mixtures

Bernardo Antunes[1,2‡], **Caroline Zanchi**[1‡], **Paul R. Johnston**[1,3,4], **Bar Maron**[2], **Christopher Witzany**[5], **Roland R. Regoes**[5], **Zvi Hayouka**[2]*, **Jens Rolff**[1,3]*

1 Freie Universität Berlin, Evolutionary Biology, Berlin, Germany, **2** Institute of Biochemistry, Food Science and Nutrition, The Hebrew University of Jerusalem, Rehovot, Israel, **3** Berlin Centre for Genomics in Biodiversity Research, Berlin, Germany, **4** University of St. Andrews, School of Medicine, North Haugh, St Andrews, Fife, United Kingdom, **5** Institute of Integrative Biology, ETH Zurich, Zurich, Switzerland

‡ These authors share first authorship on this work.
* zvi.hayouka@mail.huji.ac.il (ZH); jens.rolff@fu-berlin.de (JR)

Citation: Antunes B, Zanchi C, Johnston PR, Maron B, Witzany C, Regoes RR, et al. (2024) The evolution of antimicrobial peptide resistance in *Pseudomonas aeruginosa* is severely constrained by random peptide mixtures. PLoS Biol 22(7): e3002692. https://doi.org/10.1371/journal.pbio.3002692

Academic Editor: Kathryn Holt, London School of Hygiene & Tropical Medicine, UNITED KINGDOM

Received: February 26, 2024

Accepted: May 28, 2024

Published: July 2, 2024

Data Availability Statement: All data are available from the Zenodo database (https://doi.org/10.5281/zenodo.11209304).

Funding: This work was funded by the Joint Berlin-Jerusalem Postdoctoral Fellowship Program offered by the Freie Universität Berlin (FUB) and Hebrew University of Jerusalem (HUJI) to BA. The project was further supported by a grant from the Volkswagen Foundation (grant no. 96517) to JR. CZ was funded by the DFG (FOR 5026). The

Abstract

The prevalence of antibiotic-resistant pathogens has become a major threat to public health, requiring swift initiatives for discovering new strategies to control bacterial infections. Hence, antibiotic stewardship and rapid diagnostics, but also the development, and prudent use, of novel effective antimicrobial agents are paramount. Ideally, these agents should be less likely to select for resistance in pathogens than currently available conventional antimicrobials. The usage of antimicrobial peptides (AMPs), key components of the innate immune response, and combination therapies, have been proposed as strategies to diminish the emergence of resistance. Herein, we investigated whether newly developed random antimicrobial peptide mixtures (RPMs) can significantly reduce the risk of resistance evolution in vitro to that of single sequence AMPs, using the ESKAPE pathogen *Pseudomonas aeruginosa* (*P. aeruginosa*) as a model gram-negative bacterium. Infections of this pathogen are difficult to treat due the inherent resistance to many drug classes, enhanced by the capacity to form biofilms. *P. aeruginosa* was experimentally evolved in the presence of AMPs or RPMs, subsequentially assessing the extent of resistance evolution and cross-resistance/collateral sensitivity between treatments. Furthermore, the fitness costs of resistance on bacterial growth were studied and whole-genome sequencing used to investigate which mutations could be candidates for causing resistant phenotypes. Lastly, changes in the pharmacodynamics of the evolved bacterial strains were examined. Our findings suggest that using RPMs bears a much lower risk of resistance evolution compared to AMPs and mostly prevents cross-resistance development to other treatments, while maintaining (or even improving) drug sensitivity. This strengthens the case for using random cocktails of AMPs in favour of single AMPs, against which resistance evolved in vitro, providing an alternative to classic antibiotics worth pursuing.

funders had no role in study design, data collection and analysis, decision to publish, or preparation of the manuscript.

Competing interests: The authors have declared that no competing interests exist.

Abbreviations: AMP, antimicrobial peptide; DDW, double distilled water; DMSO, dimethyl sulfoxide; GLMM, generalised linear mixed-effect model; MM, linear mixed effect model; LPS, lipopolysaccharide; MALDI-TOF-MS, matrix-assisted laser desorption ionisation–time of flight mass spectrometry; MCMC, Markov chain Monte Carlo; MDR, multi-drug resistant; MH, Mueller–Hinton; MIC, minimum inhibition concentration; MRSA, methicillin-resistant *Staphylococcus aureus*; MSW, mutant selection window; QS, quorum sensing; RP-HPLC, reversed-phase high-performance liquid chromatography; RPM, random antimicrobial peptide mixture; SCV, small colony variant; SPPS, solid-phase peptide synthesis; TFA, trifluoroacetic acid; TIPS, triisopropylsilane; VRE, vancomycin-resistant *Enterococci*.

Introduction

The prevalence of antibiotic-resistant pathogens has become a major threat to public health, with an estimated 4.95 million deaths associated with drug-resistant bacteria in 2019 [1]. Although resistance is a natural development, misuse and overuse of antibiotics has accelerated evolutionary selection and resistance, decreasing the efficiency of available antibiotics [2,3]. Hence, there is a strong incentive to discover new strategies to control bacterial infections, such as antibiotic stewardship and rapid diagnostics, but also the development, and prudent use, of novel effective antimicrobial agents [4,5]. An important and desirable feature of such agents would be a much lower risk to select for drug resistance in pathogens than currently available conventional antimicrobials. This would make the use of such drugs much more sustainable.

Antimicrobial peptides (AMPs) form an important component of the innate immune response in multicellular organisms and have been frequently proposed as new antimicrobial drug candidates [6]. Various families of AMPs feature spatially explicit hydrophobic and cationic residues, which promote their ability to disrupt bacterial membranes [7,8]. Fundamentally, while hydrophobic residues interact with the hydrophobic interior of the lipid bilayer, their high net cationic charge selects prokaryotic membranes over eukaryotic cells [9,10]. AMPs range across the tree of life, showing a surprising diversity and variety in size and form [11]. Moreover, while resistance has been shown to evolve against these antimicrobial agents, it evolves at a much slower rate than conventional antibiotics [12–14]. Interestingly, for colistin, an AMP of bacterial origin that has been used for more than 60 years [15], it took around 50 years between the introduction and the spread of resistance [16].

In the current antibiotic crisis, bacterial pathogens are increasingly resistant to the available monotherapeutical antibiotic drugs, often evolved through redundant mechanisms and to multiple antibiotics in the same organism [17]. This situation has been exacerbated by misuse and lack of innovation in the discovery of new, and effective, antibiotic agents [18]. Hence, combination therapies have been explored and shown, by multitarget engagement, to diminish the emergence of spontaneous resistance [19,20]. Among novel strategies under scrutiny is the usage of newly developed random antimicrobial peptide mixtures (RPMs) [21,22].

The broad molecular diversity of AMPs suggests that their biological activity results from a balance of factors and is not directly coupled to sequence and/or secondary, or tertiary, structures of these peptides [8]. Hence, research groups have developed novel approaches to synthesise RPMs, using a solution containing defined concentrations of hydrophobic and cationic amino acids [21,23]. This results in 2^n peptide sequences (where n is the number of coupling steps and the chain length of the peptides). These random peptide libraries, composed of hydrophobic and cationic amino acids, have shown strong antimicrobial activity against multiple gram-negative and positive bacteria, including multi-drug resistant (MDR), methicillin-resistant *Staphylococcus aureus* (MRSA), vancomycin-resistant *Enterococci* (VRE), *Listeria monocytogenes*, and several plant pathogenic bacteria [24–27]. Moreover, some attention has been given to a subfamily of AMPs with strong antimicrobial activity—lipopeptides. Lipopeptides are produced non-ribosomally in bacteria and fungi, consisting of a short linear or cyclic peptide sequence to which a fatty acid moiety is covalently attached at the N-terminus [28]. Synthetic ultrashort lipopeptides have shown broad antimicrobial activity towards human pathogenic yeast, fungi, and bacteria, as well as plant pathogenic fungi and bacteria [29,30]. RPMs of synthetic lipopeptides have also been studied by Topman-Rakover and colleagues displaying broad antimicrobial activity against gram-negative and gram-positive bacteria, without causing cytotoxicity to mammalian cells or plants [25,26].

Here, we studied whether a treatment strategy based on the usage of RPMs and lipo-RPMs can significantly reduce the risk of resistance evolution in vitro, compared to AMPs. Our hypothesis was that RPMs, as a cocktail of multiple AMPs, represents an increased set of

Table 1. Antimicrobial peptide sequences, mode of action, and antimicrobial activity against the ancestral strain. Modes of action represented as "N/A" are not available, as they were not studied.

AMP/RPM	Sequence	Mode of action	MIC (μg/ml)
Melittin	GIGAVLKVLTTGLPALISWIKRKRQQ	Toroidal	50
Pexiganan	GIGKFLKKAKKFGKAFVKILKK	Toroidal	12,5
Cecropin P1	SWLSKTAKKLENSAKKRISEGIAIAIQGGPR	Carpet	6,25
PA-13	KIAKRIWKILRRR	Barrel stave	25
SLM1	p-KKKKK	N/A	12,5
SLM3	p-KKKFK	N/A	12,5
p-FdK5	p-F/dK 5-mer (1:1)	N/A	100
p-FdK5 (20/80)	p-F/dK 5-mer (1:4)	N/A	50
FK20	F/K 20-mer (1:1)	Barrel stave	200

AMP, antimicrobial peptide; MIC, minimum inhibition concentration; RPM, random antimicrobial peptide mixture.

https://doi.org/10.1371/journal.pbio.3002692.t001

challenges for bacteria to overcome compared to single AMPs, potentially delaying resistance evolution. The evolution of resistance in *P. aeruginosa 14* (PA14) was investigated against 9 antimicrobials: 6 single sequence AMPs and 3 RPMs, with diverse modes of action, all active against PA14 (by standard MIC assays; Table 1).

We used the ESKAPE pathogen *Pseudomonas aeruginosa* (*P. aeruginosa*) as a model gram-negative bacterium [31]. This opportunistic pathogen is involved in chronic respiratory infections, particularly those associated with cystic fibrosis, as well as hospital-acquired infections [32]. *P. aeruginosa* infections are difficult to treat due the inherent resistance to many drug classes, enhanced by the capacity to form sessile microcolonies that stick to a surface and each other, eventually forming biofilms [33,34]. Resistance associated *P. aeruginosa* deaths were estimated around 300 thousand in 2019 [1].

We allowed *P. aeruginosa* to experimentally evolve in the presence of AMPs or RPMs. The selection covered 4 weeks, which is consistent with treatment regimens of *P. aeruginosa* infections [35]. At the end of the experimental evolution course, we measured the extent of resistance evolution and whether the evolved strains showed cross-resistance/collateral sensitivity to the AMPs and RPMs. We also assessed the fitness costs of resistance on bacterial growth and used whole-genome sequencing to investigate which mutations could be candidates for causing resistant phenotypes. Finally, we investigated changes in the pharmacodynamics of the evolved bacterial strains [12,36,37]. Such a comprehensive approach has previously only been applied to a suite of single antibiotics [38] and to a small set of AMPs including a single combination [39].

The usage of random peptide libraries (i.e., RPMs) instead of homogeneous peptides (i.e., 1 sequence, 1 chain length, and 1 stereochemistry) offers some practical advantages, as the chemical synthesis of sequence-specific oligomers is more difficult and expensive than copolymerization [21]. Hence, this study aims not only to provide in-depth insight on RPMs as novel alternatives to classical antibiotics, but also to how they fare in comparison to single sequence AMPs. Our findings suggest that using RPMs results in a much lower probability of resistance evolution and mostly prevents cross-resistance development to other treatments, while maintaining (or even increasing) drug sensitivity.

Results

1. RPMs slow down resistance evolution

The level of resistance was determined based on the change of the MIC of the evolved strains in comparison to the previously determined MIC of the ancestor strain ("MIC fold-change";

Table 1). The selection regime was found to influence MIC fold-changes across the different evolved strains ($X^2_{17.88} = 565.4$; $p < 0.0001$; Figs 1 and S5). We found that all AMPs select for resistance when compared to their respective control (i.e., MIC fold-change is significantly different from the MIC fold-change of the control, when exposed to the same AMP). Among the RPMs, only p-FdK5 20/80 showed a significant difference compared to the control. The magnitude of the difference between evolved and control is much lower for the 3 RPMs compared to all the single sequence AMPs.

Additionally, under this experimental setting, the resistance to Cecropin P1 seems to evolve readily, as the control strain showed a significantly higher MIC fold-change when exposed to Cecropin P1 than in any other AMPs/RPMs-exposed control. The opposite effect can be seen in the FK20 treatment, in which the control strain shows the lowest MIC fold-change.

Overall, FK20 out-performed all the other peptides in hindering resistance evolution, including both 5-mer lipo-RPMs p-FdK5, and p-FdK5 20/80. Among single sequence AMPs, PA-13 and SLM1 performed best, leading to a lower MIC fold-change compared to the other AMPs. Post hoc analysis shows that RPMs reduce resistance evolution better than single sequence AMPs (S5 Fig), particularly evident for FK20-evolved strains.

2. Most evolved strains display collateral sensitivity to FK20

In the case of cross-resistance, evolution of resistance to one drug can increase bacterial fitness to other drugs, while the opposite is known as collateral sensitivity [40,41]. To investigate this in our experimentally evolved strains, they were exposed to the other antimicrobials of our panel (Fig 2). Across the board, strains evolved against Melittin, Pexiganan, Cecropin P1, and PA13 retained sensitivity to FK20, as did strains evolved in the presence of FK20. Furthermore, Cecropin P1-evolved strains, despite being resistant to Cecropin P1, did not show cross-resistance towards Melittin, Pexiganan, and PA-13. On the other hand, strains evolved in the presence of Melittin and Pexiganan, PA13, and FK 20 were cross-resistant to Cecropin P1, the most resistant strains being the ones evolved in the presence of Melittin and Pexiganan.

Cross-resistance/collateral sensitivity of bacterial strains evolved in the presence of lipopeptides against other lipopeptides of our panel (SLM1, SLM3 and lipo-RPMs p-FdK5 and p-

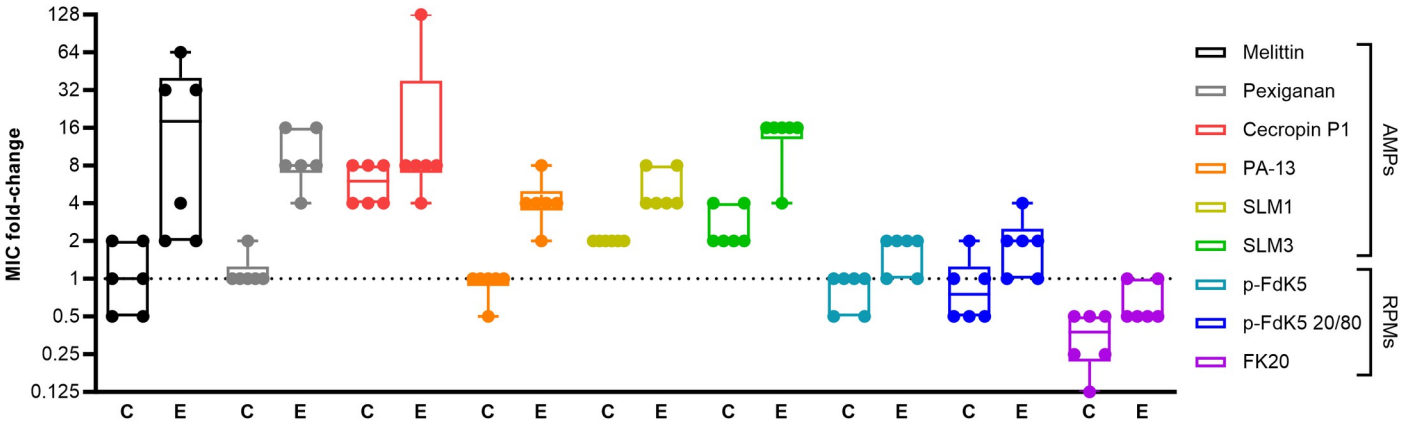

Fig 1. Resistance evolves slower against RPMs, when compared with single sequence AMPs. Resistance determined by MIC assays of each evolved strain towards the corresponding peptide ("C" indicates the MIC data of the control strain exposed to the given AMP/RPM but having be transferred in parallel during serial passages in the absence of AMP/RPM, whereas "E" indicates MIC data of the strains exposed to the given AMP/RPM, having evolved in presence of the same AMP/RPM). Results shown as log2 fold-change of the ancestor MICs. The boxes span the range between the 25th and 75th percentile, while the horizontal line inside represents the median value. The vertical bars extend to the minimum and maximum score, excluding outliers ($n = 6$; $X^2_{17,88} = 565,4$; $p < 0.0001$). The results represent 2 independent experiments. The data underlying this figure can be found in https://doi.org/10.5281/zenodo.11209304. AMP, antimicrobial peptide; MIC, minimum inhibition concentration; RPM, random antimicrobial peptide mixture.

https://doi.org/10.1371/journal.pbio.3002692.g001

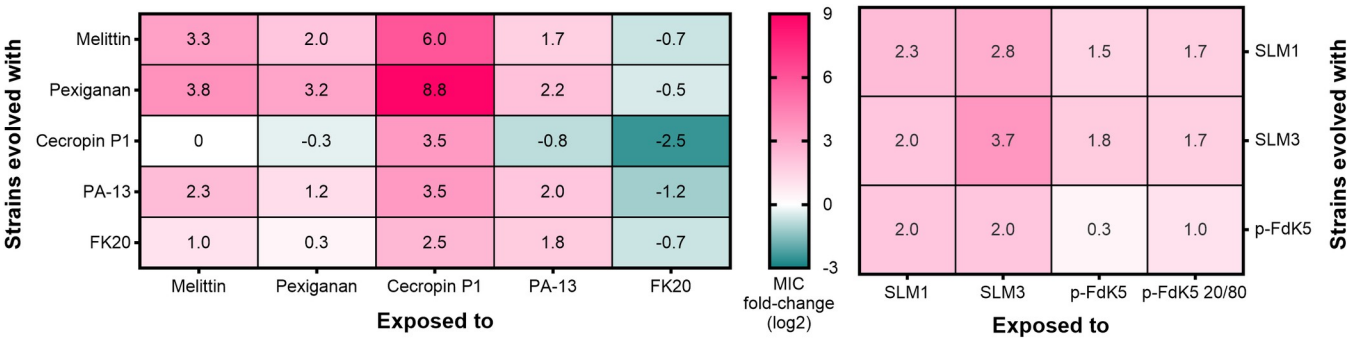

Fig 2. Cross-resistance evolved frequently against Cecropin P1, collateral sensitivity evolved rarely, but always towards FK20. A standard MIC assay was performed to evaluate whether selection in the presence of an AMP/RPM was associated to cross-resistance and/or collateral sensitivity to other AMPs/RPMs. Left panel: strains evolved in the presence of the Melittin, Pexiganan, Cecropin P1, PA13, and FK20 were exposed to each one of these 5 peptides. Right panel: strains evolved in the presence of palmitic-acid modified peptides SLM1, SLM3, and p-FdK5 were exposed to each one of these 3 peptides, plus p-FdK5 20/80. The MIC values are represented as the mean fold-change (log2) of the ancestor's MIC. The results represent 2 independent experiments ($n = 6$). Red colour represents cross-resistance and green indicates collateral sensitivity. AMP, antimicrobial peptide; MIC, minimum inhibition concentration; RPM, random antimicrobial peptide mixture.

https://doi.org/10.1371/journal.pbio.3002692.g002

FdK5 20/20) was also evaluated. We detected no observable collateral sensitivity towards the remaining palmitic acid-modified peptides (Fig 2). Nonetheless, despite great amino acid sequence similarity between peptides (Table 1), only moderate levels of cross-resistance were observed for lipo-AMPs/-RPMs. Nonetheless, the level of cross-resistance between palmitic acid modified peptides is of far lesser magnitude than the level of cross-resistance towards Cecropin P1 exhibited by strains selected for other peptides.

3. Lower resistance evolution leads to extended lag time

The fitness cost associated with the evolution of PA14 in presence, or absence, of AMP/RPMs was investigated and the parameters, lag time and maximum growth rate (Vmax), were normalised to those of the ancestor strain (i.e., fold-change; S1 Fig). There was a significant effect of the selection regime on the lag time fold-change (S1A Fig; $X^2_{9,40} = 44{,}31$; $p < 0.0001$), namely, Pexiganan-, PA-13-, SLM3-, and FK20-evolved strains display significantly increased lag times, compared to control strains (S1A and S6 Figs). There was, however, no effect of the experimental evolution regime on the maximum growth rate (Vmax) of the strains (S1B Fig; $X^2_{9,40} = 11{,}9$; $p = 0.22$).

4. Mutations evolved in all treatments

To better understand the mechanisms responsible for resistance evolution (or absence thereof), the genomic DNA of evolved strains was sequenced and compared to the assembled genome of the ancestor strain of PA14. A heat-map summary of the emerged mutations in evolved strains (including control) can be found in S2 Fig. Sequencing revealed that the majority of occurring SNPs were present in 5 genes (84%): *lasR*, *phoQ*, *tpbB*, *oprL*, and *wbpA* (Fig 3; strains without mutations were also plotted for comparison). In this section, cross-resistance/collateral sensitivity data was used to explore whether the SNPs in these 5 genes were associated with resistance to the panel of tested antimicrobials. Specifically, we tested whether presence/absence of an SNP, in each of the 5 genes, explained MIC fold-changes towards individual antimicrobial treatments, among the bacterial strains of all selection regimes. Interestingly, among these 5 genes, *tpbB* and *oprL* presented SNPs in only one of the 2 replicates of the experiment. Additionally, the software tool Provean was used to predict whether an amino acid substitution, or indel, affected the biological function of the target protein [42].

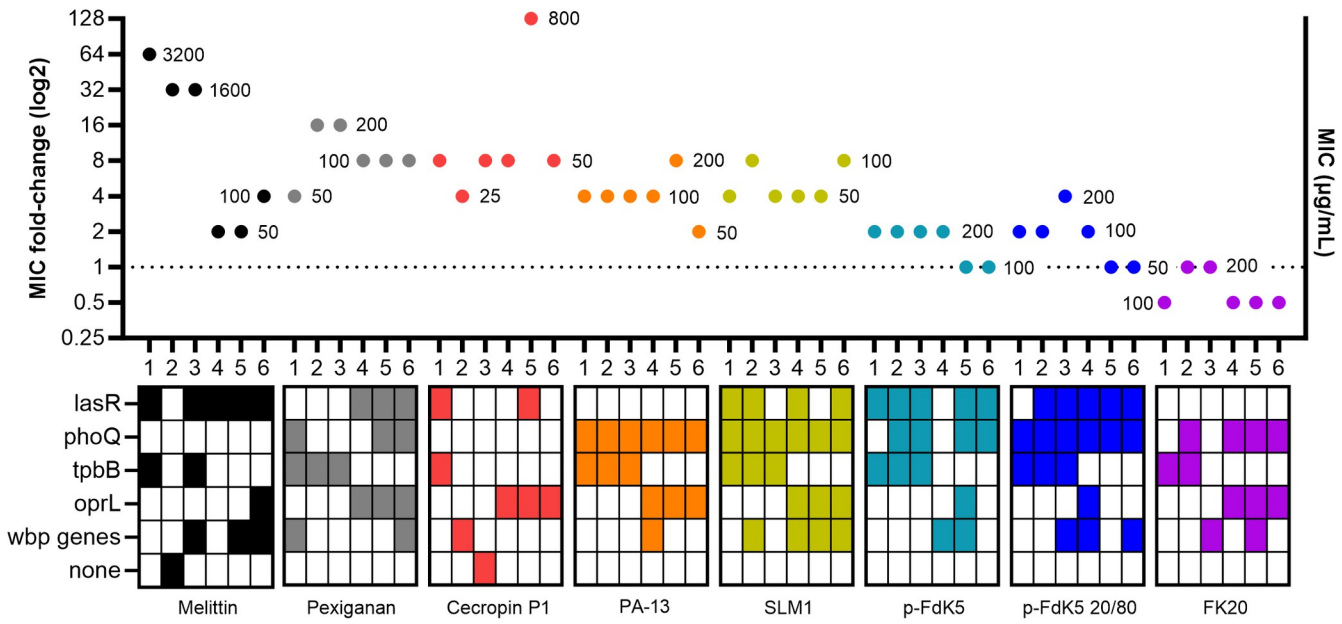

Fig 3. Representation of the resistance evolution (MIC fold-changes) in relation to the presence/absence of mutations in the 5 most frequently mutated genes. Results shown as log2 fold-change of the ancestor MICs. Each dot represents the mean of triplicates (values beside the dots represent the MIC value). The x-axis displays individual strains per treatment and the respective mutations (or absence of) are portrayed underneath. The results represent 2 independent experiments. Evolved mutations against FK20 did not result in resistant strains. The data underlying this figure can be found in https://doi.org/10.5281/zenodo.11209304. MIC, minimum inhibition concentration.

https://doi.org/10.1371/journal.pbio.3002692.g003

TpbB is a diguanylate cyclase which is directly involved in the formation small colony variants (SCVs) in *P. aeruginosa* [43]. A single type of SNPs was found in the *tpbB* gene, resulting in an amino acid substitution (valine to alanine in position 40), deemed not to affect protein function by Provean. *TpbB* gene mutations only evolved in the strains of the first replicate of the experiment, but across most of them (22 out of 27 sequenced strains), and across all treatments, including the control. Within the first replicate of the experiment, the presence of this SNP in *tpbB* did not explain MIC fold-change towards any of the tested antimicrobials (S8 Fig and S2 Table).

On the other hand, SNPs in the *oprL* gene, a membrane lipoprotein which plays an important role in the interaction of *P. aeruginosa* with the environment [44], evolved only in strains of the second replicate of the experiment. SNPs in *tpbB*, in the *orpL* gene they were found in most strains (20 out of 27), and across all treatments including the control. Unlike *tpbB*, however, SNPs found in *oprL* (leucine replaced by a phenylalanine in position 43) are predicted to impair protein function. Thus, the presence of this SNP increased MIC fold-change towards Melittin and Cecropin P1 (S9 Fig and S2 Table).

LasR is a transcriptional regulator that controls the expression of virulence factors and biofilm formation in *P. aeruginosa* [45]. In our experiments, we found a high number of different SNPs in the *lasR* gene, for most selection regimes, accounting for 27 different SNPs across 29 strains. SNPs in *lasR* were also present in 3 out of the 6 control strains. Among these 27 different SNPs, only 6 were deemed not to affect protein function by Provean, whereas the rest were deleterious. Despite this feature, the presence, or absence, of SNPs in the *lasR* gene is not associated with fold-changes in MIC towards any of the tested antimicrobials (S10 Fig and S2 Table).

We also found SNPs in several members of the *wbp* pathway leading to the synthesis of the B-band O-antigen of the lipopolysaccharide (LPS) in *P. aeruginosa* [46]. The most commonly

found SNP was a frameshift variant of *wbpA*, while the second most commonly found was a missense mutation in *wbpA*, leading to the replacement of a valine in position 32 by a glycine. The 3 SNPs found in *wbpL* also caused frameshifts, as did the 4 SNPs present in the *wbpI* gene. According to Provean, all these SNPs were deleterious, thus inactivating the products of the respective genes. It has been shown that any missing member of this pathway led to a loss of the B-band O-Antigen of LPS in *P. aeruginosa* [47]. Since, *wbp* SNPs found herein were deemed deleterious, we consider these together as inactivating the *wbp* pathway (named "*wbp* genes" in the figures; S11 Fig). Nonetheless, we did not find these deleterious SNPs to affect MIC fold-change towards any of the tested antimicrobials (S11 Fig and S2 Table). Additionally, given that such SNPs were present in all treatments, including the control, once again indicates that they were unlikely to have been selected by our antimicrobials.

Among the 5 majorly found gene mutations, only *phoQ* did not show any SNPs in the control group. The *phoQ* gene codes for a Mg^{2+} sensor which is part of a two-component system that controls several pathogenic properties in gram-negative bacteria [48]. In our experiments, the most represented SNP in *phoQ* (in 28 strains out of 29) leads to a replacement of a valine in position 260 by a glycine, which was previously associated to colistin resistance in *P. aeruginosa* isolates [49]. All SNPs were deemed deleterious by Provean.

The *phoQ* gene mutation was, in fact, the most frequently observed mutation (present in 29 different strains), although its distribution was not consistent throughout all the evolved strains. While SNPs were present in all the strains evolved in the presence of PA13, SLM1, and p-FdK5 20/80, in 4 out of 6 of the p-FdK5 and FK20-selected strains and in 3 out of 6 of Pexiganan-selected strains, they were absent from Melittin and Cecropin P1-selected strains, as well as the control strains. Moreover, the presence of this SNP in *phoQ* is associated to a higher MIC fold-change towards PA13, SLM1, SLM3, p-FdK5, and p-FdK5 20/80 (S12 Fig and S2 Table).

There were only 3 strains in which no SNPs were detected compared to the ancestor PA14: 1 in the Melittin, 1 in the Cecropin P1, and 1 in the control selection regimes (Figs 3 and S4). However, both the Melittin- and Cecropin P1-evolved strains showed a higher resistance towards Melittin and Cecropin P1, respectively. Moreover, it would have perhaps been expected to find more than just one mutation-less strain in the control group, as it was evolved absent of AMP/RPMs. Nonetheless, naturally occurring mutations result of continuous culturing are expected [50,51], and, in fact, wild-type PA14 was shown to have a 6.12×10^{-4} spontaneous mutation rate per genome [52].

Since we previously found an effect of the selection regime on the duration of the lag time, we next investigated whether this could be associated to the SNPs found in the 5 main genes.

Strains showing SNPs in the *lasR* genes had a significantly shorter lag time compared to strains which did not show any ($X^2_{1,50} = 30.79$; $p < 0.0001$). More precisely, the variance in the duration of the lag time of the strains carrying SNPs in *lasR* is greatly reduced compared to strains which have a functional *lasR* gene product (Fligner–Killeen test for homogeneity of variances: med $X^2_{1,50} = 18.862$, $p < 0.0001$; S13 Fig). This is not the case in strains carrying SNPs in *tpbB* ($X^2_{1,50} = 2.6$; $p < 0.11$), *oprL* ($X^2_{1,50} = 0.4$; $p = 0.53$), *wbp* genes ($X^2_{1,50} = 0.23$; $p = 0.63$) (S13 Fig). There is however a strong trend for the occurrence of SNPs in *phoQ* to increase the lag time of the strains ($X^2_{1,50} = 3.63$; $p = 0.057$; S13 Fig), suggesting a fitness cost to the inactivation of the *phoQ* gene product.

5. The Hill coefficient evolves with the MIC

The steepness of the pharmacodynamic curves (i.e., the Hill coefficient, kappa; κ) generated from time-kill curves provide information about the width of the mutant selection window

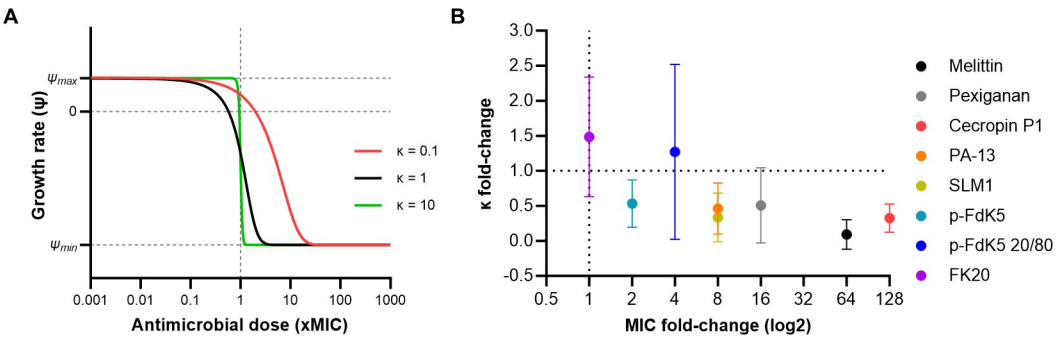

Fig 4. (A) Schematic illustration of the 4 parameters predicted by the Hill function: zMIC, ψ_{max}, ψ_{min}, and κ. The zMIC is estimated by the lowest concentration that inhibits the growth of the whole treated bacterium population. While ψ_{max} represents the maximal growth rate of bacteria (i.e., in absence of antimicrobials), ψ_{min} represents the minimal bacterial growth rate, or maximal killing rate of the antimicrobial treatment. The Hill coefficient, κ, predicts the shape and slope of the pharmacodynamic curve; the higher κ is, the steeper the pharmacodynamic curve. Pharmacodynamic curves are represented in different colours (i.e., red, black, and green) to portray the change in slope and MIC values. (B) The MIC and Hill coefficient (κ) of selected strains seem to evolve in correlational fashion. Graphic representing the correlation between evolution of resistance evolution and kappa (ρ = −0,8743; *p*-value = 0,0045). Resistance determined by MIC assay of each strain toward the corresponding peptide, shown as log2 fold-change of the ancestor MICs. Evolution of kappa determined by Hill function-based Rstan model, shown as fold-change of the ancestor's kappa. Each dot represents the mean of triplicates. The data underlying this figure can be found in https://doi.org/10.5281/zenodo.11209304. MIC, minimum inhibition concentration.

https://doi.org/10.1371/journal.pbio.3002692.g004

(i.e., the concentration range where resistant mutants are selected for; MSW), as a higher kappa results in a narrower MSW (Fig 4A). Therefore, we analysed kappa evolution for the most resistant strains, in each selection regime, by correlating it with their respective MIC fold-change (Fig 4B). The kappa value of the most resistant evolved strains was normalised to that of the ancestor, for each AMP/RPM. Six out of 8 AMP/RPMs can be found in the lower-right quadrant of MIC fold-change and kappa fold-change correlation (Fig 4B), therefore not only evolving resistance to PA14, but also generating a lower kappa than that of the ancestor strain. Indeed, a Spearman's correlation shows an inverse relationship between MIC and kappa fold-change (ρ = −0.8743; *p*-value = 0.0045), where a lower kappa correlates to a higher MIC, except for p-FdK5-evolved strains.

Using p-FdK5 20/80, despite evolving resistance, generated a slightly higher κ compared to that of the ancestor strain, therefore maintaining the sensitivity towards the evolved strains. As previously seen (Fig 1), only under FK20 selection could resistance evolution not be observed, during the 4 weeks under selection, yet it resulted in a higher kappa compared to that of the ancestor (Fig 4B).

Discussion

The present work was primarily motivated by a growing necessity and interest in exploring novel alternatives to conventional antibiotics. By using a combined approach of experimental evolution, pharmacodynamic modelling, and genome re-sequencing, we show how novel random peptide libraries compare to single AMPs in respect to antimicrobial resistance evolution. AMPs have been gaining attention for their potential as antimicrobial agents, partly because of the low probability of resistance evolution [7,8,10,53]. In fact, the WHO reported that 15.2% of antibacterials in the preclinical pipeline are AMPs [54], a notable increase from 10.7% reported in the previous review [55].

Having selected a broad array of AMPs and RPMs, shown to be active against PA14 via MIC determination (Table 1), we saw that resistance evolved against the great majority (2- to

128-fold MIC increase; Fig 1). These observations are consistent with previous evidence showing that despite lower probability of resistance evolution against AMPs compared to conventional antibiotics, in vitro resistance evolution towards AMPs can evolve [13,56,57]. Conversely, it was observed that random peptide libraries (RPMs), based on cationic and hydrophobic moieties, can significantly delay, or avoid, resistance evolution when compared to single sequence AMPs (Figs 1 and S5). While palmitic acid-modified RPMs, p-FdK5 and p-FdK5 20/80, were able to greatly reduce the magnitude of resistance evolution, FK20 was the only one effectively escaping it within the context of our experimental setting (Fig 1). The selection setting herein used covered 4 weeks, which is consistent with treatment regimens of *P. aeruginosa* infections [35].

Random peptide libraries encase a cocktail of AMPs. Whereas FK20, a 20-mer, can produce over 1 million AMP combinations (2^{20}), p-FdK5 and p-FdK5 20/80, although modified with palmitic acid for increased hydrophobicity, being 5-mers, provide less AMP combination possibilities (32 and less, respectively) [21,22,26]. Hence, the availability of a cocktail of multiple AMPs seems to favour the usage of RPMs, as it creates an increased set of challenges for bacteria to overcome, which can potentially delay resistance evolution. However, drug combinations (including AMPs) should be carefully planned, to avoid the risk of leading to formulations that are inferior to using single agents. Pena-Miller and colleagues make an interesting case when trying to achieve optimal synergistic effects in drug combinations [58]: synergy can exert strong selection for resistance, leading to consistent antagonistic emergence. Thus, unless super-inhibitory doses are applied until the pathogen is successfully cleared, synergistic antibiotics could have the opposite effect and lead to increased pathogen load. Interestingly, resistance to Cecropin P1, and to a lesser extent SLM1 and SLM3, was present in the control strain (having gone through serial passages in the absence of AMPs/RPMs). This could be explained by the reduced lag time of the strains carrying SNPs in the *lasR* gene. This would mean that the observed MIC fold-change would be the result of an improved growth of the strains and not due to the development of resistance to Cecropin P1, SLM1 and SLM3. These antimicrobials might not be efficient enough to compensate for an improved growth. Also, resistance might also be the result of a combination of mutations whose effect we could not test for because of their rarity. This higher fitness of control strains was not seen in another study involving experimental evolution towards AMPs [39]. How widespread it is, has, to the best of our knowledge, not been investigated.

Analysis of the cross-resistance/collateral sensitivity results (Fig 2) revealed some interesting patterns. Cecropin P1-evolved strains show collateral sensitivity to Pexiganan, PA-13 and FK20. Conversely, Pexiganan, PA-13 and FK20-evolved strains show cross-resistance to Cecropin P1. Remarkably, all evolved strains show collateral sensitivity to FK20, which could potentially lead to a positive impact on single AMPs if combined with FK20. In fact, several studies have proposed collateral sensitivity as a promising strategy to slow down the resistance evolution process and even reverse the preexisting resistance [41,59–61]. Imamovic and collaborators demonstrated that resistance evolution to *P. aeruginosa* for antibiotics used in cystic fibrosis patients caused collateral sensitivity to other antibiotics [41]. The study showed that the optimised drug treatment, based on the collateral sensitivity interactions, effectively eradicated the resistant subpopulation from the patient's lungs.

In line with previous studies, growth parameters lag time and maximum growth rate (Vmax) were used to estimate cost of resistance evolution [14,62]. Our investigation revealed that strains evolved in the presence of Pexiganan, PA-13, SLM3, and FK20 displayed a fitness cost, resulting in significantly increased lag times compared to control (S1A Fig). This result is surprising in the case of FK20-evolved strains, which did not evolve resistance. There were no differences between the lag time of the ancestor and the procedural controls after selection

(S1A Fig), thus adaptation to the experimental conditions did not affect this aspect of the bacterial fitness. Ward and associates [63] have shown that, clinically isolated MDR strains of *P. aeruginosa* frequently have similar fitness in the absence of antibiotics. Therefore, under certain circumstances, using AMP formulations against which resistance evolution is more costly, might be more effective in preventing resistance evolution, though the relationship between cost and resistance is not always strong [64].

No selection regime significantly affected Vmax compared to control, however, the Vmax of the control groups was higher than that of the ancestor (S1B Fig). Faster growth rates than that of the ancestor strain have been shown to result from adaptation to a serial passaging environment [65,66], due to an enhanced ability to acquire, or more efficiently utilise available nutrients during post-exponential growth. On the other hand, no significant differences in Vmax were found between experimentally evolved strains, in either treated or control regimes (S1B Fig). A study that induced bacterial resistance to Tachyplesin I (including in *P. aeruginosa*) similarly revealed that resistance acquisition did not markedly affect Vmax, in comparison to the control, but did extend the lag phase [67]. The authors argue that AMP resistance might compromise bacterial fitness in different ways, not necessarily affecting the maximum growth rate.

We further studied which mutations evolved in our experimental selection treatments. By finding new mutations that emerge in parallel, independently propagated lines of bacterial strains exposed to antibiotics in controlled environments, are likely the cause of new heritable resistant genotypes [68]. Among the 5 genes comprising most of the SNPs in our dataset, *phoQ* was the only one for which SNPs did not evolve in the control lines, suggesting that it evolved as a response to a selection pressure exerted by some of the antimicrobials of our panel. This SNP results in the substitution of a valine by a glycine in position 260 (Histidine kinase A domain), which was deemed to abolish protein function by Provean. This same SNP has also been previously reported to lead to loss-of-function of the PhoQ protein, leading to an increased resistance to colistin in *P. aeruginosa* by Lee and Ko [49].

In *P. aeruginosa*, adaptive resistance to cationic AMPs is known to occur in response to limiting extracellular concentrations of Mg^{2+} and Ca^{2+} cations [69,70]. This adaptation is controlled by two-component regulators PhoP-PhoQ and PmrA-PmrB which up-regulate the expression of the *arnBCADTEF* LPS modification operon [70]. The products of these *arn* genes lead to reducing the net negative charge of LPS, limiting the interaction and self-promoted uptake of polycationic antibiotics (e.g., AMPs and aminoglycosides). *PhoQ* expression allows for the integration of environmental cues when bacterial density is high and nutritional resources are rarefied [71]. Inactivation of *phoQ* ultimately lead to constitutive LPS modifications which have been shown to confer *P. aeruginosa* colistin resistance [72].

PhoQ SNPs were present in all evolved treatments, except Melittin and Cecropin P1-selected strains. Moreover, the presence of this SNP in *phoQ* is associated to a higher MIC fold-change towards PA13, SLM1, SLM3, p-FdK5, and p-FdK5 20/80, but not towards Melittin, Cecropin P1, and Pexiganan (S12 Fig). Although SNPs in *phoQ* were selected for in the strains evolved in the presence of Pexiganan, they were never selected for in strains evolved in the presence of Melittin and Cecropin P1, which opens another line of evidence in favour of SNPs in *phoQ* being under selection by the pressure exerted by some antimicrobials. Murphy and colleagues [73] showed that the exposure to AMPs and RPMs, instead of resulting in repeatable modifications of LPS, resulted in a change in the relative proportions of different LPS species at the surface of the bacterial membrane. This makes us unable to predict how this SNP in *phoQ* would affect interactions of AMPs/RPMs with the membrane and/or between AMP/RPM molecules, and more functional studies would be needed to elucidate on why *phoQ* mutations do not affect resistance to some antimicrobials. Interestingly, given that *phoQ*

SNPs were not found in Melittin and Cecropin P1-evolved strains, the only antimicrobial-selected group with the *phoQ* mutation, which was not associated with higher MIC fold-change is FK20. We did not detect any further SNPs in the *arn* operon or in the *phoP* gene. Environmental conditions were kept constant in our experiments, and selected lines were always exposed to antimicrobials. One could thus expect that the inactivation of PhoQ, being an environmental sensor upstream of the cascade leading to LPS modifications, leading to constitutive LPS modifications, to be a more efficient to achieve resistance in our setting. On the other hand, the resistance phenotype of PhoP null mutants is conditional to the concentration of Mg^{2+} in the environment (67), and it has been shown that mutants of the *phoP* gene achieve a lower degree of resistance compared to *phoQ* mutants (47). SNPs found in the 4 other genes (*lasR*, *wbp* genes, *tpbB*, and *oprL*) were also detected in the strains of the control selection regime, which means that antimicrobials are unlikely to have selected for their emergence in our bacterial strains.

We found a high number of different SNPs in the *lasR* gene (mostly predicted to be deleterious) in the bacterial strains, although the presence of these SNPs did not affect MIC fold-change towards any of the tested antimicrobials in our experimental setting (S10 Fig). LasR has been shown to play an important role in resistance evolution as part of *P. aeruginosa* quorum sensing (QS) [74]. The *P. aeruginosa* QS circuitry is comprised of at least 2 complete systems, LasR–LasI and RhlR–RhlI [75]. Here, the transcriptional regulator LasR controls the expression of virulence factors, such as elastase LasB17, exotoxin A, pyocyanin and EPS, important players for resistance evolution in *P. aeruginosa* [76]. Notably, polymorphic populations of *P. aeruginosa* comprising various mutants for *lasR* are selected first in patients with chronic obstructive pulmonary disease [77]. Yet, despite this crucial involvement in resistance, accumulation of SNPs in the *lasR* gene have been shown to be widespread in *P. aeruginosa* isolated from various environments, and in the absence of a distinct selection pressure [78]. These previous findings are confirmed in our present study, however, the reduced lag time and variance in lag time of strains carrying an SNPs in *lasR* suggests that they confer a fitness benefit to the strains. This benefit might explain the presence of SNPs in *lasR* even in the absence of selection pressure exerted by antimicrobials, as a result of an adaptation to optimise growth in our experimental conditions. Interestingly, SNPs in *lasR* were absent from strains evolved in the presence of PA13 and FK20, which might indicate a constraint on quorum sensing function imposed by these 2 antimicrobials during evolution.

The biosynthesis of the B-band O-antigen of LPS is product of genes in the *wbp* pathway, among which are *wbpA*, *wbpI*, and *wbpL* [79]. The loss of one gene product in this pathway leads to loss-of-function of the B-band O-antigen at the cell surface [47]. We found all SNPs in *wbpA*, *wbpI*, and *wbpL* (named "*wbp* genes") to be deleterious, thus it is likely that in our experiments the bacterial strains presenting such an SNP do not possess the B-band O-antigen of LPS. This molecule has been shown to play a critical role in host colonization, providing resistance to both serum sensitivity and phagocytosis [80–82], whereas mutants of *P. aeruginosa* deficient in O-antigen synthesis are sensitive to the killing effects of human serum-mediated lysis [83].

With the emergence of mucoid *P. aeruginosa* within the lungs of CF patients, there are cell surface changes with respect to LPS phenotype, characterized by minor expression or complete lack of B-band O-antigen, while the level of A-band is maintained [81]. Once *P. aeruginosa* has colonised the lungs, these LPS modifications are probably beneficial for evasion of host defences (A band is less immunogenic) and for alteration of susceptibility to antibiotics, since loss of B-band O-antigen confers resistance to aminoglycosides [84]. Thus, given that we found *wbp* pathway SNPs in every evolved treatment, including the control, and that they do not explain MIC fold-change, one could propose that these gene mutations resulted from an

adaptation to a biofilm environment, rather than from selection by the panel of antimicrobials tested.

We found an SNP in the tpbB gene (also called yfiN), coding for a diguanylate cyclase which regulates the output of messenger cyclic-di-GMP (c-di-GMP) [85], in only one of the 2 experimental blocks (S8 Fig). Several *Pseudomonas* strains (including PA14) undergo phenotypic diversification while adapting to the biofilm environment, forming SCVs [85]. Strong evidence has linked SCVs formation to elevated levels of messenger cyclic-di-GMP (c-di-GMP), associated with sessile phenotypes, expressing biofilm formation and attachment factors [86]. Resistant *P. aeruginosa* SCVs phenotype have been shown to inactivate *yfiR* and *tpbA*, negative regulators of *tpbB*, leading to increased biofilm production [87]. In our experimentally evolved strains, the SNP in *tpbB* was found to be neutral, which might explain why no effect of this SNP on the MIC-fold change was detected towards any of the tested antimicrobials (S8 Fig).

SNPs in the *oprL* gene were also present in all selection regimes, but only in the second replicate of the experiment. They consist of a leucine substitution by a phenylalanine in position 43, leading to protein inactivation. OprL is the second most abundant outer membrane protein in *P. aeruginosa*, equivalent of the *E. coli* peptidoglycan-associated lipoprotein [88]. Together with small lipoprotein OprI, OprL interacts with peptidoglycans, maintaining cell integrity [88], offering protection from oxidative stress [89], and contributing to antibiotic resistance mechanisms in *P. aeruginosa* by adjusting membrane permeability and multidrug efflux pumps, which secrete the drugs directly out of the cell [90]. In the experimentally evolved strains of this study, the presence of this deleterious SNP in the *oprL* gene correlated with a higher MIC fold-change towards Melittin- and Cecropin P1-evolved strains (S9 Fig).

Altogether, our data points to the efficiency of FK20 to slow down, or prevent, the magnitude of resistance evolution of *P. aeruginosa*. A rationale to consider is that FK20 is a random peptide library of over 1 million sequences, making it very difficult to evolve resistance and hence resistance evolution against FK20 was not discovered within the four-week selection time span in our experiment. In fact, the goal of using multiple antimicrobials would be to achieve a combined effect, leading to killing efficacy and/or resistance avoidance, superior to the sum of their individual counterparts (i.e., synergistic interaction) [37]. Synergy between AMPs is common, leading to increased killing efficacy, while constraining resistance evolution, which could explain their combinational occurrence in nature [6,91,92]. Albeit molecular mechanisms of interactions of AMPs are still largely unknown [6], pore-forming peptides can assist other coapplied transmembrane AMPs to quickly invade bacterial cells and substantially interrupt the metabolism [93].

Insight on why antimicrobial resistance against AMPs evolves with low probabilities, or in the case of FK20 with extremely low probabilities, relies on the molecular mechanisms of killing, but also on the investigation of pharmacodynamics in vitro, such as the one portrayed herein and by others [6,39] and in vivo [94]. Our study revealed that AMP resistance evolution in *P. aeruginosa* resulted in increased MICs, except for FK20, but also that the Hill coefficient, kappa, evolves as well [36]. Kappa (κ) describes how sensitive the bacterial populations net growth rate is to changes in antimicrobial concentration. High κ values represent steeper pharmacodynamic curves (i.e., for concentrations close to the MIC, a small increase in concentration leads to a big decrease in net growth). Therefore, for high κ values a given antibiotic substance (e.g., random peptide libraries or AMP combinations) has a narrower range of concentrations exerting selection on resistant bacteria over susceptible ones [6,37]. This leads to the idea that kappa might relate to the probability of resistance evolution against AMPs [12].

A negative correlation between MIC fold-change and kappa fold-change revealed that, generally, lower resistance evolution led to steeper pharmacodynamic curves (i.e., kappa; Fig 4B).

Similarly, El Shazely and colleagues have previously shown a proof-of-concept study illustrating that kappa evolves in *S. aureus* [39]. How kappa and the actual AMP-membrane interactions are related in our examples, and in fact in most, requires further study. Work by Srinivasan and colleagues has studied and summarised possible mechanisms including cooperativity, oligomerization, and aggregation of AMP molecules [95].

Yu and colleagues have shown that MIC and kappa significantly varied between single AMPs and AMP combinations [6]. As numbers of AMPs increased in combination, the MIC of the combinations decreased and, reversibly, kappa increased. Random peptide libraries are combinations of multiple random AMP sequences, a feature that might be crucial and hold potential for outperforming combinations of a few single AMPs.

The mutant selection window (MSW) is defined as the range of antimicrobial concentrations where the resistant mutants are selectively favoured over susceptible strains [96]. The upper bound is given by the MIC of the resistant mutant, the lower bound, also known as the minimal selective concentration [97], is reached when the net growth rates of the resistant and susceptible strains are equal. By using random peptide libraries, such as FK20, that lead to higher kappa values, in comparison to single AMP-evolved strains, could narrow the range of concentrations selecting resistance (i.e., the MSW).

Conclusions

This work reinforced the idea of combinational therapy as a path for tackling antibiotic resistance, highlighting the potential therapeutical capacity of random peptide libraries. Herein, a 20-mer random peptide library, FK20, was shown to avoid resistance and remain sensitive after selection, despite evolving mutations and fitness costs. Our findings suggest that *P. aeruginosa* detects the presence of these antimicrobial agents, but for the duration of our in vitro selection protocol (i.e., 4 weeks), were not able to evolve effective resistance mechanisms. Additionally, these cationic and hydrophobic AMP cocktails can be synthesised affordably and have shown to be nontoxic and nonhaemolytic in a mouse model [21,22]. The findings herein depicted strengthen the case for favouring the usage of random cocktails of AMPs over single AMPs, against which resistance evolved in vitro.

In the past, promising studies have claimed novel antibiotics "resistance-proof," able to stay effective at killing their target pathogens, such as the case of Teixobactin [98], being later refuted [99]. Thus, despite the positive findings herein evidenced for FK20, one should side with caution. Moreover, further studies should be conducted concerning the interaction of these RPMs with the host innate immunity. The usage of AMPs/RPMs that strongly synergize with host innate immune response should be favoured, as it could lead to an overall reduction in dosage, hence reducing potential side effects [100]. A synergistic strategy involving random peptide libraries and the host immune response holds potential to be a cost-efficient way to reduce bacterial loads and avoid resistance evolution.

Materials and methods

Bacterial strains and growth conditions

All experiments were performed with the *P. aeruginosa* 14 strain (PA14; kindly provided by Yael Helman) [101]. This strain is defined as the ancestor strain. Prior to each experiment, strains were plated on Mueller–Hinton (MH) agar plates (HiMedia), and individual colonies were picked and grown in MH broth overnight at 37˚C. All bacterial cells used in this study were stored in 25% glycerol at −80˚C.

Synthesis of antimicrobial peptides

Six different AMPs and 3 RPMs were selected for experimental evolution (Table 1). In addition to the peptides developed in house (i.e., SLM1, SLM3, p-FdK5, p-FdK5 20/80, and FK20; [22,25,26]), 4 additional AMPs were selected. Melittin is the major protein component of the venom of the European honeybee (*Apis mellifera*) [102]. Pexiganan is a synthetic analog of magainin peptides, isolated from the skin of the African clawed frog [103]. Cecropin P1 was isolated from the parasitic nematode *Ascaris suum*, found in pig's intestine [104]. PA-13 is a short synthetic alpha-helical hybrid peptide, inspired by cathelicidin and aurein [105]. While SLM1 and SLM3 are specific palmitic acid-modified 5-mer peptides, composed of L-Lysine and/or L-Phenylalanine, part of a 32-peptide library, p-FdK5 and p-FdK5 20/80 are randomised 5-mers, using L-Phenylalanine and D-Lysine (to the ratios of 1:1 and 1:4, respectively; S1 Fig) [25,26]. Lastly, FK20 was synthetized as random peptide of L-Phenylalanine and L-Lysine (1:1 ratio) [22].

All peptides were synthesised by 9-fluorenylmethoxy carbonyl (Fmoc) solid-phase peptide synthesis (SPPS), using a peptide synthesizer (Liberty Blue; CEM, United States of America). To generate lipo-RPMs and SLMs, acylation was produced by bounding palmitic acid to the N-terminus of the desired peptide/RPM, using the same Fmoc chemistry, albeit that overnight shaking, at room temperature, was used instead of microwave irradiation [26]. Upon synthesis completion, peptides were, sequentially, cleaved from the resin (95% trifluoroacetic acid [TFA], 2.5% water, and 2.5% triisopropylsilane [TIPS]), resuspended in double distilled water (DDW), frozen, and lyophilized. The resulting crude peptide was dissolved in dimethyl sulfoxide (DMSO) and purified by semipreparative reversed-phase high-performance liquid chromatography (RP-HPLC), while matrix-assisted laser desorption ionisation–time of flight mass spectrometry (MALDI-TOF-MS) was utilised for verification of the peptide mass and purity. RPMs containing phenylalanine and lysine (FK20, pFdK5, pFdK5 20/80) were synthesised as previously described [21].

Minimum inhibition concentration (MIC) determination

MIC values were determined following a standard serial dilution protocol, as described elsewhere [27]. Briefly, PA14 cells were grown overnight in MH broth, at 37˚C and 200 rpm. Subsequently, cells were diluted 1:100 in MH broth and grown until reaching an optical density at 595 nm (OD_{595}) of 0.1. Then, 100 μl of 5×10^5 CFU/ml were inoculated into each well in 96-well plates that contained a serial dilution of AMPs or RPMs. Each plate contained 3 replicate lines per peptide. The MICs were defined as the lowest concentration at which there was inhibition of bacterial growth by at least 90%, after 24 h, by measuring the OD_{595}.

The MIC was determined on 3 occasions: (1) prior to the experiment, to determine the concentration of our focal peptides to be used at the start of the experimental evolution (i.e., MIC of the ancestor strain); (2) at the end of the experimental evolution, detect an increase, or decrease, in the resistance of the experimentally evolved strains to our peptides of interest; (3) to evaluate whether the experimental evolution of a certain treatment was accompanied by an increase, or decrease, in resistance or sensitivity to another antimicrobial (i.e., cross-resistance or collateral-sensitivity).

Due to time constrains, the design of the cross-resistance/collateral sensitivity experiments are not full factorial, instead, we focussed on comparisons we found most relevant: (1) we exposed strains evolved in the presence of the AMPs Melittin, Pexiganan, Cecropin P1 and PA13, and the RPM FK20 to each other; (2) we then exposed strains evolved in the presence of palmitic acid-modified peptides to peptides of the same family, namely SLM1-, SLM3-, and p-FdK5-evolved strains to SLM1, SLM3, p-FdK5, and p-FdK5 20/80.

The MIC of evolved strains was divided by MIC of the ancestor to determine the respective fold-change in comparison to the ancestor (see "Statistical analysis" section).

Experimental evolution procedure

Prior to evolution with AMPs/RPMs, a PA14 colony was transferred from an MH agar plate into 5 ml MH broth in a 50 ml tube and incubated overnight, at 37˚C and 200 rpm. Subsequently, this starter culture was diluted 20-fold into a 1.5 ml Eppendorf tube containing 850 μl MH broth to maintain the same headspace ratio of 96-well plates, used in the experimental evolution procedure, and incubated, overnight, under the same conditions (37˚C and 200 rpm). This process was repeated for 7 transfers to adapt the bacteria to the experimental conditions.

The experimental evolution procedure was designed to exert selective pressure while avoiding extinction of bacterial lines, as previously described [27]. Each line was exposed to 4 concentrations of AMP/RPMs, according to their MIC, as follows: 1.5×, 1×, 0.5×, and 0.25× (Table 1). All AMP/RPMs were dissolved in DDW, except for FK20, which was dissolved in 10% DMSO (which translates to a working 0.5% working concentration). Experiments were performed in 96-well plates, and each AMP/RPM had 3 parallel replicates (sharing the same ancestral inoculum). Each plate included 8 wells with bacteria absent of AMPs/RPMs, as a positive control, as well as 4 wells with just medium, as negative control. Daily, 10 μl of the previous plate was transferred into 190 μl of fresh medium and AMPs. Every 4 days, bacteria from the highest concentration of AMP/RPM were selected and transferred into 4 concentrations in the new plate. MIC was doubled when growth was observed in 4 out of 6 lines at the MIC or higher. The experimental evolution was carried out for 27 transfers (approx. 114 generations). Before every selection or MIC increment, samples were taken for fossil record in 25% glycerol stocks and preserved at −80˚C to avoid line extinction. Spot plating was performed on MH agar, containing 5 μg/ml tetracycline, to confirm growth before selection. Experimental evolutions were performed twice, yielding 6 replicates per selection regime over 2 replicates of the experiment. The strains of the first replicate of the experimental evolution experiment originated from a single colony, while the strains of the second replicate, performed later, originate from a different single colony.

Fitness cost of evolved strains

Bacterial cells were grown overnight in MH broth and then diluted to an OD_{595} of 0.1. For each strain, 200 μl of culture were transferred into 96-well plates, with 3 technical replicates. Optical density (OD595) was measured every 15 min for 24 h using an Epoch 2 microplate reader (BioTek). Lag time and Vmax were assessed using the plate reader software (Gen5). The values measured in the experimentally evolved strains were divided by the values of their respective ancestors and expressed as lag time fold-change and Vmax fold-change (see "Statistical analysis" section).

DNA isolation

Genomic DNA for whole-genome sequencing was isolated using GeneMATRIX Bacterial and Yeast genomic DNA purification kit (Roboklon, Germany) following manufacturer's instructions. Four μl of 10 mg/ml freshly prepared lysozyme and lysostaphin (both from Sigma) each were added into bacterial lysate. The DNA quantity and quality were estimated by measuring the optical density at A260/280 using the Nanodrop spectrophotometer (Thermo Scientific) and the Qubit 4 Fluorometer (Thermo Scientific).

Sequencing

At the end of each replicate of the experimental evolution experiment, 10 μl of the content of each well was plated on MH agar and incubated overnight. One single colony was picked per plate/well to be re-sequenced. As a reference genome, we used a de novo assembly of a single colony of PA14 taken from our frozen stock (after overnight culture).

The library of the ancestor strain was sequenced on a minion (Oxford Nanopore Technologies, Oxford), at 400 bps translocation speed, using a kit 14 chemistry flowcell, and the resulting raw sequencing data were basecalled using Guppy model dna_r10.4.1_e8.2_400bps_sup. Sequencing reads were adaptor trimmed using porechop [106] and filtered using filtlong [107] to retain approximately 150-fold coverage comprising reads of at least 1,000 bp. The filtered reads were assembled using flye [108], which produced a single circular contig that was further polished using medaka consensus [109]. The remaining errors were corrected using illumina reads together with polypolish [110]. Finally, the start position of the assembly was adjusted to begin at dnaA using circlator [111]. The result was annotated with prokka [112].

Endpoint re-sequencing of the evolved strains was done on an Illumina HiSeq2000 with 100 bp paired-end reads (Wellcome Trust Centre for Human Genetics, Oxford, United Kingdom). The sequencing data had a mean depth of 35.9× and a mean coverage of 76.4% at 30× depth. Sequencing Adaptors were trimmed with trimmomatic [113]. Snippy [114] was used to call variants using by default parameters, with the annotated assembly described above as a reference sequence. The Provean software tool was used to predict the effect of SNPs on the function of their target protein, namely amino acid substitution or indels [42].

Killing curves

AMP/RPM-selected strains were serially diluted (2-fold concentration gradient), starting from 10× MIC, in 96-well plates. Approximately, 2–3 × 10^6 log-phase bacteria were added to a total volume of 100 ml. The plates were incubated at 37˚C. As it is known that AMP-mediated killing is quick [115,116], dose-response was monitored within 60 min [6]. To do so, 10 μl of bacterial suspension were sampled after 5, 10, 20, 40, and 60 min, then immediately diluted in 90 μl PBS and plated on square solid MHA plates. These solid agar plates were transferred into a 37˚C incubator and incubated for 24 h before counting CFUs. The same procedure was followed to assess killing curves for the sensitive ancestor PA14 strain. The assays were performed in triplicates.

Modelling killing curves—Pharmacodynamics

Pharmacodynamics captures the functional relationship between drug dosage and bacterial growth or death. To model the killing curve, describing the relationship between the concentration of AMPs/RPMs and the killing and/or growth rate of the exposed bacteria, the Hill function was used [36]. This function estimates 4 parameters: zMIC, κ, ψ_{min}, and ψ_{max} (Fig 4A). The zMIC is the MIC estimated by fitting; κ, the Hill coefficient, depicts the steepness of the curve relating bacterial growth to drug concentration; ψ_{min}, and ψ_{max} represent the minimum and maximum growth rates of bacteria, respectively (see Hill function equations in S1 Supplementary methods). Growth rate and killing rate of bacteria are estimated from the time-kill curves as the change of CFU over time by using generalized linear regression. The data for CFU were all log transformed. The starting point of linear regression was the first measurement. We then fitted the growth rate and killing rate with eq 4 (see S1 Supplementary methods), based on the Markov chain Monte Carlo (MCMC) method and generated the pharmacodynamic curves. Pharmacodynamic parameters of the most resistant experimentally evolved strains and ancestor were estimated and a summary can be found in S1 Table.

Statistical analysis

All the data was analysed using the R software [117] and figures of the main text were produced using GraphPad Prism, version 9 for Windows, GraphPad Software, Boston, Massachusetts, USA.

We normalised the MICs of the different evolved strains generated in this series of experiments (as well as the control strain) by dividing them with the MIC of their respective ancestors, which represents the MICs before applying the selection regime. The resulting variable is a fold-change in MIC ("MIC fold-change") at the end of the experimental evolution compared to the beginning.

Similarly, we normalised both fitness readouts duration of the lag phase (lag time) and maximum slope of the bacterial growth curve (Vmax) to the readouts of the ancestor of the given evolved strain by dividing the values of the evolved strains to that of their respective ancestors. The resulting variable is a fold-change in Vmax and lag time during experimental evolution: Vmax fold-change and lag time fold-change.

These response variables are therefore ratios, which are non-integer despite representing count data. They showed the dispersion typical of count data, as well as a heterogeneity in the variances between treatments. MIC fold-changes had a maximum of 3 digits after the comma. They were multiplied by 1,000 to analyse them with models fitted for a negative binomial distribution (see details below), since this distribution assumes a positive and integer response variable. We multiplied the lag time fold-change by 100 and rounded it up according to the value of the third digit after the comma to perform a similar analysis. However, such was not the case for the Vmax fold-change data which satisfied the assumptions of a linear mixed model and did not require to be multiplied and rounded.

We then analysed the MIC and lag time fold-change of single sequence AMPs and RPMs strains, generated by experimental evolution, with a generalised linear mixed-effect model (GLMM), fitted for a negative binomial distribution, according to the selection regime. Since the MIC fold-change was always assessed towards the antimicrobial used, as a selection pressure during experimental evolution, there was no further need to include the antimicrobial towards which the MIC was measured with as an explanatory variable. Since the whole experiment was replicated in 2 experimental blocks, we included this experimental block as a random factor. We used the "glmmTMB" function of the "glmmTMB" package [118]. As stated above, we analysed the Vmax fold-change of the resulting strains with a linear mixed effect model (LMM, "lmer" function of the "lme4" package) [119], including Vmax fold-change as a response variable according to the selection regime and the experimental block as a random factor.

Pairwise comparisons between selection regimes can be performed by eye, as previously reported [120,121]: the difference between 2 selection regimes is deemed significant when the 95% confidence intervals (95CI) do not overlap more than half of their length. Effect plots for post hoc comparison between different selection regimes (estimates of the models with the corresponding 95CIs) are displayed in the Supporting information (S5–S7 Figs), which were generated with the "effects" package [122,123].

Additionally, we analysed whether the lag time was explained by presence or absence of SNPs in 5 genes by fitting 1 GLMM (negative binomial distribution) per gene, with lag time × 100 being the response variable and according to presence or absence of SNP in the focal gene as the explanatory variable, with the block as a random factor ("glmmTMB" function of the "glmmTMB" package; S13 Fig).

We next used the cross-resistance/collateral sensitivity dataset to analyse whether the presence, or absence, of SNPs in the 5 genes which concentrated most of the SNPs (*lasR*, *wbp*

genes, *phoQ*, *tpbB*, and *oprL*) affected the MIC fold-changes in the bacterial strains. We built the following model for each gene/antimicrobial combination: MIC fold-change ×1,000 as a response variable explained by presence/absence of SNP in a gene, and the experimental block as a random factor ("glmmTMB" function of the "glmmTMB" package). Since SNPs in *tpbB* and *oprL* only emerged in strains from 1 of the 2 experimental blocks, we performed this analysis only in the replicate in which SNPs were present, using the "glm.nb" function of the "MASS" package [124]. We considered all bacterial strains, regardless of their selection regime of origin, since the selection regime, which affects the presence, or absence, of SNPs in the strains, would have been colinear with the latter. The box plots representing the data are provided in the Supporting information (S5–S7 Figs) and were produced with the "ggplot2" and "ggpubr" packages [125,126].

Correlation between kappa fold-change and MIC fold-change was assessed using Spearman's test (ρ), which estimates a rank-based measure of association, through the "cor.test" function included in the "stats" package [127].

Pharmacodynamics analyses were performed using Rstan [128].

Supporting information

S1 Table. Pharmacodynamic parameters (zMIC, κ, ψmin, and ψmax) for the ancestor and most resistant evolved strains, acquired by fitting time-kill curves to the Hill function using Rstan.
(DOCX)

S2 Table. Summary of the results of the GLMMs (GLMs in the case of the tpbB and oprL genes, for which SNPs were present only in 1 replicate of the experiment, thus not requiring a random factor), performed across strains of several selection regimes, by testing the influence of SNPs in several genes on the magnitude of resistance evolution. One model was fitted to each gene/antimicrobial combination. The explanatory variable is the presence, or absence, of a SNP in the focal gene (regardless of the selection regime the strain originated from), and the response variable is the MIC fold-change to the various antimicrobials of interest: presence/absence of SNPs in gene~MIC fold-change. The Chi square with degrees of freedom (X^2df,ddf) is given on top, the *p*-value on the bottom. The cells of the table containing no results (-) are the combinations of SNP and antimicrobial for which there was only 1 bacterial strain showing no SNP in the given gene, therefore not allowing for a proper comparison. The models for which the presence of SNP in the focal gene significantly influenced the MIC fold-change have their results written in bold.
(DOCX)

S1 Fig. Fitness cost of individual peptide evolved strains, determined by growing the bacteria in the absence of AMPs and normalised to that of the ancestor. OD595 was measured every 15 min through 24 h. (A) Lag time ($n = 6$; $X^2$9,40 = 44,31; $p < 0.0001$); (B) maximum growth rate (Vmax; $n = 6$; $X^2$9,40 = 11,9; $p = 0.22$). The boxes span the range between the 25th and 75th percentile, while the horizontal black line inside represents the median value. The vertical bars extend to the minimum and maximum score, excluding outliers. The results represent 2 independent experiments. The data underlying this figure can be found in https://doi.org/10.5281/zenodo.11209304.
(DOCX)

S2 Fig. Heat map of mutations obtained from whole-genome sequencing, using the ancestor PA14 as reference.
(DOCX)

S3 Fig. Relation between resistance evolution (MIC fold-change) and all gene mutations assessed by whole-genome sequencing. Resistance determined by MIC assay of each strain toward the corresponding peptide. Results shown as log2 fold-change of the ancestor MICs. Each dot represents the mean of triplicates. The data underlying this figure can be found in https://doi.org/10.5281/zenodo.11209304.
(DOCX)

S4 Fig. Representation of the resistance evolution of control strains (MIC fold-changes) in relation to the presence/absence of mutations in the 5 most frequently mutated genes. Resistance determined by MIC assay of each strain toward the corresponding peptide. Results shown as log2 fold-change of the ancestor MICs. Each dot represents the mean of triplicates (values beside the dots represent the MIC value). The x-axis displays individual strains per treatment and the respective mutations (or absence of) are portrayed underneath. The results represent 2 independent experiments. The data underlying this figure can be found in https://doi.org/10.5281/zenodo.11209304.
(DOCX)

S5 Fig. Plot displaying the coefficients (dots) with 95CIs (vertical bars) of the negative binomial GLMM analysing MIC fold-change, according to the selection regime as a focal predictor, including an experimental block as a random factor. The x-axis represents the antimicrobial used as a selection pressure during experimental evolution of the bacterial strains, as well as for assessment of their MIC fold-change (see colour code in the guide on the right side of the plot). The y-axis is a non-linear scale of the MIC fold-change multiplied by 1,000, to be integer and satisfy assumptions for a negative-binomial GLMM. Full dots represent coefficients for the strain selected against the assessed antimicrobial, whereas open dots represent the coefficient for the control strain, serially passaged in the absence of antimicrobial and tested against the antimicrobial of interest. A significant difference between treatment levels is observed when 95CI do not overlap on more than half of their length (see "Statistical analysis" section). The data underlying this figure can be found in https://doi.org/10.5281/zenodo.11209304.
(DOCX)

S6 Fig. Plot displaying the coefficients (dots) with 95CIs (vertical bars) of the negative binomial GLMM analysing the lag time fold-change (in the absence of antimicrobial), according to the selection regime as a focal predictor, including an experimental block as a random factor. The x-axis represents the antimicrobial used as a selection pressure during experimental evolution of the bacterial strains (see colour code in the guide on the right side of the plot). The y-axis represents the lag time fold-change multiplied by 100, rounded to be integer and satisfy assumptions for a negative-binomial GLMM. A significant difference between treatment levels is observed when 95CI do not overlap on more than half of their length (see "Statistical analysis" section). The data underlying this figure can be found in https://doi.org/10.5281/zenodo.11209304.
(DOCX)

S7 Fig. Plot displaying the coefficients (dots) with 95CIs (vertical bars) of the LMM analysing the Vmax fold-change (in the absence of antimicrobial), according to the selection regime as a focal predictor, including an experimental block as a random factor. The x-axis represents the antimicrobial used as a selection pressure during experimental evolution of the bacterial strains (see colour code in the guide on the right side of the plot). The y-axis represents the Vmax fold-change. A significant difference between treatment levels is observed

when 95CI do not overlap on more than half of their length (see "Statistical analysis" section). The data underlying this figure can be found in https://doi.org/10.5281/zenodo.11209304.
(DOCX)

S8 Fig. Boxplots representing the MIC fold-change towards several antimicrobials, according to the presence, or absence, of tpbB gene SNPs (across strains from different selection regimes). The antimicrobial to which the bacterial strains were exposed to, is given in the window of the boxplot. On the x-axis: absence (0) or presence (1) of tpbB gene SNPs. On the y-axis: MIC fold-change of experimental evolution. The boxes span the range between the 25th and 75th percentile, while the horizontal black line inside represents the median value. The vertical bars extend to the minimum and maximum score, excluding outliers. The individual datapoints represent the MIC fold-change of 1 bacterial strain carrying an SNP. SNPs in the tpbB gene emerged only in 1 replicate of the experiment. The boxplots representing MIC fold changes towards Melittin, Pexiganan, Cecropin P1, PA13, and FK20 contain the data of strains originating from the Melittin, Pexiganan, Cecropin P1, PA13, and control selection regimes. The boxplots representing MIC fold-change towards SLM1, SLM3, p-FdK5, and p-FdK5 20/80 contain the data of strains originating from the SLM1 and control treatments. In the SLM1 selection regime, only 1 strain did not show a SNP in tpbB, making the comparison between presence/absence of SNP irrelevant. The corresponding statistical tests are given in the S2 Table. The data underlying this figure can be found in https://doi.org/10.5281/zenodo.11209304.
(DOCX)

S9 Fig. Boxplots representing the MIC fold-change towards several antimicrobials, according to the presence, or absence, of oprL gene SNPs (across strains from different selection regimes). The antimicrobial to which the bacterial strains were exposed to, is given in the window of the boxplot. On the x-axis: absence (0) or presence (1) of oprL gene SNPs. On the y-axis: MIC fold-change of experimental evolution. The boxes span the range between the 25th and 75th percentile, while the horizontal black line inside represents the median value. The vertical bars extend to the minimum and maximum score, excluding outliers. The individual datapoints represent the MIC fold-change of 1 bacterial strain carrying an SNP. SNPs in the tpbB gene emerged only in 1 replicate of the experiment. The boxplots representing MIC fold changes towards Melittin, Pexiganan, Cecropin P1, PA13, and FK20 contain the data of strains originating from the Melittin, Pexiganan, Cecropin P1, PA13, and control selection regimes. The boxplots representing MIC fold-change towards SLM1, SLM3, p-FdK5, and p-FdK5 20/80 contain the data of strains originating from the SLM1 and control treatments. In the SLM1 selection regime, only 1 strain did not show an SNP in oprL, making the comparison between presence/absence of SNP irrelevant. The corresponding statistical tests are given in the S2 Table. The data underlying this figure can be found in https://doi.org/10.5281/zenodo.11209304.
(DOCX)

S10 Fig. Boxplots representing the MIC fold-change towards several antimicrobials, according to the presence, or absence, of lasR gene SNPs (across strains from different selection regimes). The antimicrobial to which the bacterial strains were exposed to, is given in the window of the boxplot. On the x-axis: absence (0) or presence (1) of lasR gene SNPs. On the y-axis: MIC fold-change of experimental evolution. The boxes span the range between the 25th and 75th percentile, while the horizontal black line inside represents the median value. The vertical bars extend to the minimum and maximum score, excluding outliers. The individual datapoints represent the MIC fold-change of 1 bacterial strain carrying an SNP, acquired

over 2 replicates of the experiment. The boxplots representing MIC fold-change towards Melittin, Pexiganan, Cecropin P1, PA13, and FK20 contain the data of strains originating from the Melittin, Pexiganan, Cecropin P1, PA13, and control selection regimes. The boxplots representing MIC fold-change towards SLM1, SLM3, p-FdK5, and p-FdK5 20/80 contain the data of strains originating from the SLM1 and control treatments. The corresponding statistical tests are given in the S2 Table. The data underlying this figure can be found in https://doi.org/10.5281/zenodo.11209304.
(DOCX)

S11 Fig. Boxplots representing the MIC fold-change towards several antimicrobials, according to the presence, or absence, of SNPs from wbp pathway genes (across strains from different selection regimes). The antimicrobial to which the bacterial strains were exposed to, is given in the window of the boxplot. On the x-axis: absence (0) or presence (1) of SNPs from wbp pathway genes. On the y-axis: MIC fold-change of experimental evolution. The boxes span the range between the 25th and 75th percentile, while the horizontal black line inside represents the median value. The vertical bars extend to the minimum and maximum score, excluding outliers. The individual datapoints represent the MIC fold-change of 1 bacterial strain carrying an SNP, acquired over 2 replicates of the experiment. The boxplots representing MIC fold-change towards Melittin, Pexiganan, Cecropin P1, PA13, and FK20 contain the data of strains originating from the Melittin, Pexiganan, Cecropin P1, PA13, and control selection regimes. The boxplots representing MIC fold-change towards SLM1, SLM3, p-FdK5, and p-FdK5 20/80 contain the data of strains originating from the SLM1 and control treatments. The corresponding statistical tests are given in the S2 Table. The data underlying this figure can be found in https://doi.org/10.5281/zenodo.11209304.
(DOCX)

S12 Fig. Boxplots representing the MIC fold-change towards several antimicrobials, according to the presence, or absence, of phoQ gene SNPs (across strains from different selection regimes). The antimicrobial to which the bacterial strains were exposed to, is given in the window of the boxplot. On the x-axis: absence (0) or presence (1) of phoQ gene SNPs. On the y-axis: MIC fold-change of experimental evolution. The boxes span the range between the 25th and 75th percentile, while the horizontal black line inside represents the median value. The vertical bars extend to the minimum and maximum score, excluding outliers. The individual datapoints represent the MIC fold-change of 1 bacterial strain carrying an SNP, acquired over 2 replicates of the experiment. The boxplots representing MIC fold-change towards Melittin, Pexiganan, Cecropin P1, PA13, and FK20 contain the data of strains originating from the Melittin, Pexiganan, Cecropin P1, PA13, and control selection regimes. The boxplots representing MIC fold-change towards SLM1, SLM3, p-FdK5, and p-FdK5 20/80 contain the data of strains originating from the SLM1 and control treatments. The corresponding statistical tests are given in the S2 Table. The data underlying this figure can be found in https://doi.org/10.5281/zenodo.11209304.
(DOCX)

S13 Fig. Boxplots representing the duration of the lag phase (lag time) in the presence or absence of SNP in the main 5 genes (5 genes harbouring most of the SNPs across strains from different selection regimes). The focal gene is given in the window of the boxplot. On the x-axis: absence (0) or presence (1) of SNPs in the gene. On the y-axis: lag time in minutes. The boxes span the range between the 25th and 75th percentile, while the horizontal black line inside represents the median value. The vertical bars extend to the minimum and maximum score, excluding outliers. The individual datapoints represent the lag time of 1 bacterial strain.

The lag time shows less variation when SNPs are present in the lasR gene of the strains, and there is a strong trend for SNPs in the phoQ gene to increase the lag time of the strains (see main text for corresponding statistical tests). The data underlying this figure can be found in https://doi.org/10.5281/zenodo.11209304.
(DOCX)

S1 Supplementary methods. Modelling killing curves—Pharmacodynamics.
(DOCX)

Acknowledgments

The authors thank E. Bittermann for the input and assistance in setting up samples for whole-genome sequencing and Ronan Murphy for critically reading the manuscript and helping with data interpretation.

Author Contributions

Conceptualization: Bernardo Antunes, Zvi Hayouka, Jens Rolff.

Data curation: Bernardo Antunes, Caroline Zanchi, Paul R. Johnston, Christopher Witzany.

Formal analysis: Caroline Zanchi, Paul R. Johnston, Christopher Witzany, Roland R. Regoes.

Funding acquisition: Zvi Hayouka, Jens Rolff.

Investigation: Bernardo Antunes, Caroline Zanchi, Paul R. Johnston, Bar Maron, Jens Rolff.

Methodology: Bernardo Antunes, Paul R. Johnston, Bar Maron, Zvi Hayouka.

Project administration: Zvi Hayouka.

Resources: Zvi Hayouka, Jens Rolff.

Software: Caroline Zanchi, Paul R. Johnston.

Supervision: Paul R. Johnston, Roland R. Regoes, Zvi Hayouka, Jens Rolff.

Validation: Caroline Zanchi, Zvi Hayouka, Jens Rolff.

Visualization: Bernardo Antunes, Caroline Zanchi.

Writing – original draft: Bernardo Antunes, Jens Rolff.

Writing – review & editing: Bernardo Antunes, Caroline Zanchi, Paul R. Johnston, Bar Maron, Christopher Witzany, Roland R. Regoes, Zvi Hayouka, Jens Rolff.

References

1. Antimicrobial Resistance C. Global burden of bacterial antimicrobial resistance in 2019: a systematic analysis. Lancet. 2022; 399(10325):629–55. https://doi.org/10.1016/S0140-6736(21)02724-0 PMID: 35065702
2. Qiu D, Ke M, Zhang Q, Zhang F, Lu T, Sun L, et al. Response of microbial antibiotic resistance to pesticides: An emerging health threat. Sci Total Environ. 2022; 850:158057. https://doi.org/10.1016/j.scitotenv.2022.158057 PMID: 35977623
3. Lepore C, Silver L, Theuretzbacher U, Thomas J, Visi D. The small-molecule antibiotics pipeline: 2014–2018. Nat Rev Drug Discov. 2019; 18(10):739. https://doi.org/10.1038/d41573-019-00130-8 PMID: 31570838
4. Organization WH. The evolving threat of antimicrobial resistance: options for action: World Health Organization; 2012.

5. Czaplewski L, Bax R, Clokie M, Dawson M, Fairhead H, Fischetti VA, et al. Alternatives to antibiotics-a pipeline portfolio review. Lancet Infect Dis. 2016; 16(2):239–51. https://doi.org/10.1016/S1473-3099(15)00466-1 PMID: 26795692

6. Yu G, Baeder DY, Regoes RR, Rolff J. Combination Effects of Antimicrobial Peptides. Antimicrob Agents Chemother. 2016; 60(3):1717–24. https://doi.org/10.1128/AAC.02434-15 PMID: 26729502

7. Zasloff M. Antimicrobial peptides of multicellular organisms. Nature. 2002; 415(6870):389–95. https://doi.org/10.1038/415389a PMID: 11807545

8. Rathinakumar R, Walkenhorst WF, Wimley WC. Broad-spectrum antimicrobial peptides by rational combinatorial design and high-throughput screening: the importance of interfacial activity. J Am Chem Soc. 2009; 131(22):7609–17. https://doi.org/10.1021/ja8093247 PMID: 19445503

9. Axelsen PH. A chaotic pore model of polypeptide antibiotic action. Biophys J. 2008; 94(5):1549–50. https://doi.org/10.1529/biophysj.107.124792 PMID: 18065456

10. Hancock RE. Cationic peptides: effectors in innate immunity and novel antimicrobials. Lancet Infect Dis. 2001; 1(3):156–64. https://doi.org/10.1016/S1473-3099(01)00092-5 PMID: 11871492

11. Rodriguez-Rojas A, Nath A, El Shazely B, Santi G, Kim JJ, Weise C, et al. Antimicrobial Peptide Induced-Stress Renders Staphylococcus aureus Susceptible to Toxic Nucleoside Analogs. Front Immunol. 2020; 11:1686. https://doi.org/10.3389/fimmu.2020.01686 PMID: 33133056

12. Yu G, Baeder DY, Regoes RR, Rolff J. Predicting drug resistance evolution: insights from antimicrobial peptides and antibiotics. Proc Biol Sci. 2018; 285(1874). https://doi.org/10.1098/rspb.2017.2687 PMID: 29540517

13. Perron GG, Zasloff M, Bell G. Experimental evolution of resistance to an antimicrobial peptide. Proc Biol Sci. 2006; 273(1583):251–6. https://doi.org/10.1098/rspb.2005.3301 PMID: 16555795

14. Spohn R, Daruka L, Lazar V, Martins A, Vidovics F, Grezal G, et al. Integrated evolutionary analysis reveals antimicrobial peptides with limited resistance. Nat Commun. 2019; 10(1):4538. https://doi.org/10.1038/s41467-019-12364-6 PMID: 31586049

15. Bian X, Qu X, Zhang J, Nang SC, Bergen PJ, Tony Zhou Q, et al. Pharmacokinetics and pharmacodynamics of peptide antibiotics. Adv Drug Deliv Rev. 2022; 183:114171. https://doi.org/10.1016/j.addr.2022.114171 PMID: 35189264

16. Liu YY, Wang Y, Walsh TR, Yi LX, Zhang R, Spencer J, et al. Emergence of plasmid-mediated colistin resistance mechanism MCR-1 in animals and human beings in China: a microbiological and molecular biological study. Lancet Infect Dis. 2016; 16(2):161–8. https://doi.org/10.1016/S1473-3099(15)00424-7 PMID: 26603172

17. Tacconelli E, Carrara E, Savoldi A, Harbarth S, Mendelson M, Monnet DL, et al. Discovery, research, and development of new antibiotics: the WHO priority list of antibiotic-resistant bacteria and tuberculosis. Lancet Infect Dis. 2018; 18(3):318–27. https://doi.org/10.1016/S1473-3099(17)30753-3 PMID: 29276051

18. Laxminarayan R, Duse A, Wattal C, Zaidi AK, Wertheim HF, Sumpradit N, et al. Antibiotic resistance-the need for global solutions. Lancet Infect Dis. 2013; 13(12):1057–98. https://doi.org/10.1016/S1473-3099(13)70318-9 PMID: 24252483

19. Tyers M, Wright GD. Drug combinations: a strategy to extend the life of antibiotics in the 21st century. Nat Rev Microbiol. 2019; 17(3):141–55. https://doi.org/10.1038/s41579-018-0141-x PMID: 30683887

20. Roemhild R, Bollenbach T, Andersson DI. The physiology and genetics of bacterial responses to antibiotic combinations. Nat Rev Microbiol. 2022; 20(8):478–90. https://doi.org/10.1038/s41579-022-00700-5 PMID: 35241807

21. Hayouka Z, Chakraborty S, Liu R, Boersma MD, Weisblum B, Gellman SH. Interplay among subunit identity, subunit proportion, chain length, and stereochemistry in the activity profile of sequence-random peptide mixtures. J Am Chem Soc. 2013; 135(32):11748–51. https://doi.org/10.1021/ja406231b PMID: 23909610

22. Hayouka Z, Bella A, Stern T, Ray S, Jiang H, Grovenor CRM, et al. Binary Encoding of Random Peptide Sequences for Selective and Differential Antimicrobial Mechanisms. Angew Chem Int Ed Engl. 2017; 56(28):8099–103. https://doi.org/10.1002/anie.201702313 PMID: 28557193

23. Siriwardena TN, Gan BH, Kohler T, van Delden C, Javor S, Reymond JL. Stereorandomization as a Method to Probe Peptide Bioactivity. ACS Cent Sci. 2021; 7(1):126–34. https://doi.org/10.1021/acscentsci.0c01135 PMID: 33532575

24. Stern T, Zelinger E, Hayouka Z. Random peptide mixtures inhibit and eradicate methicillin-resistant Staphylococcus aureus biofilms. Chem Commun (Camb). 2016; 52(44):7102–5. https://doi.org/10.1039/c6cc01438k PMID: 27161246

25. Topman S, Tamir-Ariel D, Bochnic-Tamir H, Stern Bauer T, Shafir S, Burdman S, et al. Random peptide mixtures as new crop protection agents. J Microbial Biotechnol. 2018; 11(6):1027–36. https://doi.org/10.1111/1751-7915.13258 PMID: 29488347

26. Topman-Rakover S, Malach E, Burdman S, Hayouka Z. Antibacterial lipo-random peptide mixtures exhibit high selectivity and synergistic interactions. Chem Commun (Camb). 2020; 56(80):12053–6. https://doi.org/10.1039/d0cc04493h PMID: 32902531

27. Maron B, Rolff J, Friedman J, Hayouka Z. Antimicrobial Peptide Combination Can Hinder Resistance Evolution. Microbiol Spectr. 2022; 10(4):e0097322. https://doi.org/10.1128/spectrum.00973-22 PMID: 35862981

28. Makovitzki A, Avrahami D, Shai Y. Ultrashort antibacterial and antifungal lipopeptides. Proc Natl Acad Sci U S A. 2006; 103(43):15997–6002. https://doi.org/10.1073/pnas.0606129103 PMID: 17038500

29. Makovitzki A, Viterbo A, Brotman Y, Chet I, Shai Y. Inhibition of fungal and bacterial plant pathogens in vitro and in planta with ultrashort cationic lipopeptides. Appl Environ Microbiol. 2007; 73(20):6629–36. https://doi.org/10.1128/AEM.01334-07 PMID: 17720828

30. Brotman Y, Makovitzki A, Shai Y, Chet I, Viterbo A. Synthetic ultrashort cationic lipopeptides induce systemic plant defense responses against bacterial and fungal pathogens. Appl Environ Microbiol. 2009; 75(16):5373–9. https://doi.org/10.1128/AEM.00724-09 PMID: 19542326

31. Pendleton JN, Gorman SP, Gilmore BF. Clinical relevance of the ESKAPE pathogens. Expert Rev Anti Infect Ther. 2013; 11(3):297–308. https://doi.org/10.1586/eri.13.12 PMID: 23458769

32. Stover CK, Pham XQ, Erwin AL, Mizoguchi SD, Warrener P, Hickey MJ, et al. Complete genome sequence of Pseudomonas aeruginosa PAO1, an opportunistic pathogen. Nature. 2000; 406 (6799):959–64. https://doi.org/10.1038/35023079 PMID: 10984043

33. Livermore DM. Multiple mechanisms of antimicrobial resistance in Pseudomonas aeruginosa: our worst nightmare? Clin Infect Dis. 2002; 34(5):634–40. https://doi.org/10.1086/338782 PMID: 11823954

34. Ben Hur D, Kapach G, Wani NA, Kiper E, Ashkenazi M, Smollan G, et al. Antimicrobial Peptides against Multidrug-Resistant Pseudomonas aeruginosa Biofilm from Cystic Fibrosis Patients. J Med Chem. 2022; 65(13):9050–62. https://doi.org/10.1021/acs.jmedchem.2c00270 PMID: 35759644

35. Reynolds D, Kollef M. The Epidemiology and Pathogenesis and Treatment of Pseudomonas aeruginosa Infections: An Update. Drugs. 2021; 81(18):2117–31. https://doi.org/10.1007/s40265-021-01635-6 PMID: 34743315

36. Regoes RR, Wiuff C, Zappala RM, Garner KN, Baquero F, Levin BR. Pharmacodynamic functions: a multiparameter approach to the design of antibiotic treatment regimens. Antimicrob Agents Chemother. 2004; 48(10):3670–6. https://doi.org/10.1128/AAC.48.10.3670-3676.2004 PMID: 15388418

37. Witzany C, Rolff J, Regoes RR, Igler C. The pharmacokinetic-pharmacodynamic modelling framework as a tool to predict drug resistance evolution. Microbiology (Reading). 2023; 169(7). https://doi.org/10.1099/mic.0.001368 PMID: 37522891

38. Chevereau G, Dravecka M, Batur T, Guvenek A, Ayhan DH, Toprak E, et al. Quantifying the Determinants of Evolutionary Dynamics Leading to Drug Resistance. PLoS Biol. 2015; 13(11):e1002299. https://doi.org/10.1371/journal.pbio.1002299 PMID: 26581035

39. El Shazely B, Yu G, Johnston PR, Rolff J. Resistance Evolution Against Antimicrobial Peptides in Staphylococcus aureus Alters Pharmacodynamics Beyond the MIC. Front Microbiol. 2020; 11:103. https://doi.org/10.3389/fmicb.2020.00103 PMID: 32117132

40. Pál C, Papp B, Lázár V. Collateral sensitivity of antibiotic-resistant microbes. Trends Microbiol. 2015; 23(7):401–7. https://doi.org/10.1016/j.tim.2015.02.009 PMID: 25818802

41. Imamovic L, Sommer MO. Use of collateral sensitivity networks to design drug cycling protocols that avoid resistance development. Sci Transl Med. 2013; 5(204):204ra132. https://doi.org/10.1126/scitranslmed.3006609 PMID: 24068739

42. Choi Y, Sims GE, Murphy S, Miller JR, Chan AP. Predicting the functional effect of amino acid substitutions and indels. PLoS ONE. 2012; 7(10):e46688. https://doi.org/10.1371/journal.pone.0046688 PMID: 23056405

43. Ueda A, Wood TK. Connecting quorum sensing, c-di-GMP, pel polysaccharide, and biofilm formation in Pseudomonas aeruginosa through tyrosine phosphatase TpbA (PA3885). PLoS Pathog. 2009; 5 (6):e1000483. https://doi.org/10.1371/journal.ppat.1000483 PMID: 19543378

44. Lim A, De Vos D, Brauns M, Mossialos D, Gaballa A, Qing D, et al. Molecular and immunological characterization of OprL, the 18 kDa outer-membrane peptidoglycan-associated lipoprotein (PAL) of Pseudomonas aeruginosa. Microbiology (Reading). 1997; 143(Pt 5):1709–16. https://doi.org/10.1099/00221287-143-5-1709 PMID: 9168620

45. Gambello MJ, Iglewski BH. Cloning and characterization of the Pseudomonas aeruginosa lasR gene, a transcriptional activator of elastase expression. J Bacteriol. 1991; 173(9):3000–9. https://doi.org/10.1128/jb.173.9.3000-3009.1991 PMID: 1902216

46. Burrows LL, Charter DF, Lam JS. Molecular characterization of the Pseudomonas aeruginosa serotype O5 (PAO1) B-band lipopolysaccharide gene cluster. Mol Microbiol. 1996; 22(3):481–95. https://doi.org/10.1046/j.1365-2958.1996.1351503.x PMID: 8939432

47. Larkin A, Imperiali B. Biosynthesis of UDP-GlcNAc(3NAc)A by WbpB, WbpE, and WbpD: enzymes in the Wbp pathway responsible for O-antigen assembly in Pseudomonas aeruginosa PAO1. Biochemistry. 2009; 48(23):5446–55. https://doi.org/10.1021/bi900186u PMID: 19348502

48. Fields PI, Groisman EA, Heffron F. A Salmonella locus that controls resistance to microbicidal proteins from phagocytic cells. Science. 1989; 243(4894):1059–62. https://doi.org/10.1126/science.2646710 PMID: 2646710

49. Lee JY, Ko KS. Mutations and expression of PmrAB and PhoPQ related with colistin resistance in Pseudomonas aeruginosa clinical isolates. Diagn Microbiol Infect Dis. 2014; 78(3):271–6. https://doi.org/10.1016/j.diagmicrobio.2013.11.027 PMID: 24412662

50. Heurlier K, Denervaud V, Haenni M, Guy L, Krishnapillai V, Haas D. Quorum-sensing-negative (lasR) mutants of Pseudomonas aeruginosa avoid cell lysis and death. J Bacteriol. 2005; 187(14):4875–83. https://doi.org/10.1128/JB.187.14.4875-4883.2005 PMID: 15995202

51. Perfeito L, Fernandes L, Mota C, Gordo I. Adaptive mutations in bacteria: high rate and small effects. Science. 2007; 317(5839):813–5. https://doi.org/10.1126/science.1142284 PMID: 17690297

52. Dettman JR, Sztepanacz JL, Kassen R. The properties of spontaneous mutations in the opportunistic pathogen Pseudomonas aeruginosa. BMC Genomics. 2016; 17:27. https://doi.org/10.1186/s12864-015-2244-3 PMID: 26732503

53. Mookherjee N, Anderson MA, Haagsman HP, Davidson DJ. Antimicrobial host defence peptides: functions and clinical potential. Nat Rev Drug Discov. 2020; 19(5):311–32. https://doi.org/10.1038/s41573-019-0058-8 PMID: 32107480

54. Organization WH. Antibacterial agents in clinical and preclinical development: an overview and analysis. World Health Organization; 2021.

55. Organization WH. Antibacterial agents in preclinical development: an open access database. World Health Organization; 2019.

56. Dobson AJ, Purves J, Kamysz W, Rolff J. Comparing selection on *S. aureus* between antimicrobial peptides and common antibiotics. PLoS ONE. 2013; 8(10):e76521.

57. Habets MG, Brockhurst MA. Therapeutic antimicrobial peptides may compromise natural immunity. Biol Lett. 2012; 8(3):416–8. https://doi.org/10.1098/rsbl.2011.1203 PMID: 22279153

58. Pena-Miller R, Laehnemann D, Jansen G, Fuentes-Hernandez A, Rosenstiel P, Schulenburg H, et al. When the most potent combination of antibiotics selects for the greatest bacterial load: the smile-frown transition. PLoS Biol. 2013; 11(4):e1001540. https://doi.org/10.1371/journal.pbio.1001540 PMID: 23630452

59. Baym M, Stone LK, Kishony R. Multidrug evolutionary strategies to reverse antibiotic resistance. Science. 2016; 351(6268):aad3292. https://doi.org/10.1126/science.aad3292 PMID: 26722002

60. Lazar V, Martins A, Spohn R, Daruka L, Grezal G, Fekete G, et al. Antibiotic-resistant bacteria show widespread collateral sensitivity to antimicrobial peptides. Nat Microbiol. 2018; 3(6):718–31. https://doi.org/10.1038/s41564-018-0164-0 PMID: 29795541

61. Barbosa C, Beardmore R, Schulenburg H, Jansen G. Antibiotic combination efficacy (ACE) networks for a Pseudomonas aeruginosa model. PLoS Biol. 2018; 16(4):e2004356. https://doi.org/10.1371/journal.pbio.2004356 PMID: 29708964

62. Makarova O, Johnston P, Rodriguez-Rojas A, El Shazely B, Morales JM, Rolff J. Genomics of experimental adaptation of Staphylococcus aureus to a natural combination of insect antimicrobial peptides. Sci Rep. 2018; 8(1):15359. https://doi.org/10.1038/s41598-018-33593-7 PMID: 30337550

63. Ward H, Perron GG, Maclean RC. The cost of multiple drug resistance in Pseudomonas aeruginosa. J Evol Biol. 2009; 22(5):997–1003. https://doi.org/10.1111/j.1420-9101.2009.01712.x PMID: 19298493

64. Igler C, Rolff J, Regoes R. Multi-step vs. single-step resistance evolution under different drugs, pharmacokinetics, and treatment regimens. Elife. 2021;10. https://doi.org/10.7554/eLife.64116 PMID: 34001313

65. Somerville GA, Chaussee MS, Morgan CI, Fitzgerald JR, Dorward DW, Reitzer LJ, et al. Staphylococcus aureus aconitase inactivation unexpectedly inhibits post-exponential-phase growth and enhances stationary-phase survival. Infect Immun. 2002; 70(11):6373–82. https://doi.org/10.1128/IAI.70.11.6373-6382.2002 PMID: 12379717

66. LaCroix RA, Palsson BO, Feist AM. A Model for Designing Adaptive Laboratory Evolution Experiments. Appl Environ Microbiol. 2017; 83(8).

67. Hong J, Hu J, Ke F. Experimental Induction of Bacterial Resistance to the Antimicrobial Peptide Tachyplesin I and Investigation of the Resistance Mechanisms. Antimicrob Agents Chemother. 2016; 60 (10):6067–75. https://doi.org/10.1128/AAC.00640-16 PMID: 27480861

68. Santos-Lopez A, Fritz MJ, Lombardo JB, Burr AHP, Heinrich VA, Marshall CW, et al. Evolved resistance to a novel cationic peptide antibiotic requires high mutation supply. Evol Med Public Health. 2022; 10(1):266–76. https://doi.org/10.1093/emph/eoac022 PMID: 35712084

69. Macfarlane EL, Kwasnicka A, Ochs MM, Hancock RE. PhoP-PhoQ homologues in Pseudomonas aeruginosa regulate expression of the outer-membrane protein OprH and polymyxin B resistance. Mol Microbiol. 1999; 34(2):305–16. https://doi.org/10.1046/j.1365-2958.1999.01600.x PMID: 10564474

70. McPhee JB, Lewenza S, Hancock RE. Cationic antimicrobial peptides activate a two-component regulatory system, PmrA-PmrB, that regulates resistance to polymyxin B and cationic antimicrobial peptides in Pseudomonas aeruginosa. Mol Microbiol. 2003; 50(1):205–17. https://doi.org/10.1046/j.1365-2958.2003.03673.x PMID: 14507375

71. Groisman EA. The pleiotropic two-component regulatory system PhoP-PhoQ. J Bacteriol. 2001; 183 (6):1835–42. https://doi.org/10.1128/JB.183.6.1835-1842.2001 PMID: 11222580

72. Miller AK, Brannon MK, Stevens L, Johansen HK, Selgrade SE, Miller SI, et al. PhoQ mutations promote lipid A modification and polymyxin resistance of Pseudomonas aeruginosa found in colistin-treated cystic fibrosis patients. Antimicrob Agents Chemother. 2011; 55(12):5761–9. https://doi.org/10.1128/AAC.05391-11 PMID: 21968359

73. Murphy RA, Pizzato J, Cuthbertson L, Sabnis A, Edwards AM, Nolan LM, et al. Antimicrobial peptide glatiramer acetate targets Pseudomonas aeruginosa lipopolysaccharides to breach membranes without altering lipopolysaccharide modification. NPJ Antimicrob Resist. 2024; 2(1):4.

74. Li Y, Xia L, Chen J, Lian Y, Dandekar AA, Xu F, et al. Resistance elicited by sub-lethal concentrations of ampicillin is partially mediated by quorum sensing in Pseudomonas aeruginosa. Environ Int. 2021; 156:106619. https://doi.org/10.1016/j.envint.2021.106619 PMID: 33989839

75. Gilbert KB, Kim TH, Gupta R, Greenberg EP, Schuster M. Global position analysis of the Pseudomonas aeruginosa quorum-sensing transcription factor LasR. Mol Microbiol. 2009; 73(6):1072–85. https://doi.org/10.1111/j.1365-2958.2009.06832.x PMID: 19682264

76. Sakuragi Y, Kolter R. Quorum-sensing regulation of the biofilm matrix genes (pel) of Pseudomonas aeruginosa. J Bacteriol. 2007; 189(14):5383–6. https://doi.org/10.1128/JB.00137-07 PMID: 17496081

77. Zhao K, Yang X, Zeng Q, Zhang Y, Li H, Yan C, et al. Evolution of lasR mutants in polymorphic Pseudomonas aeruginosa populations facilitates chronic infection of the lung. Nat Commun. 2023; 14 (1):5976. https://doi.org/10.1038/s41467-023-41704-w PMID: 37749088

78. Ciofu O, Mandsberg LF, Bjarnsholt T, Wassermann T, Hoiby N. Genetic adaptation of Pseudomonas aeruginosa during chronic lung infection of patients with cystic fibrosis: strong and weak mutators with heterogeneous genetic backgrounds emerge in mucA and/or lasR mutants. Microbiology (Reading). 2010; 156(Pt 4):1108–19. https://doi.org/10.1099/mic.0.033993-0 PMID: 20019078

79. Miller WL, Wenzel CQ, Daniels C, Larocque S, Brisson JR, Lam JS. Biochemical characterization of WbpA, a UDP-N-acetyl-D-glucosamine 6-dehydrogenase involved in O-antigen biosynthesis in Pseudomonas aeruginosa PAO1. J Biol Chem. 2004; 279(36):37551–8. https://doi.org/10.1074/jbc.M404749200 PMID: 15226302

80. Hancock RE, Mutharia LM, Chan L, Darveau RP, Speert DP, Pier GB. Pseudomonas aeruginosa isolates from patients with cystic fibrosis: a class of serum-sensitive, nontypable strains deficient in lipopolysaccharide O side chains. Infect Immun. 1983; 42(1):170–7. https://doi.org/10.1128/iai.42.1.170-177.1983 PMID: 6413410

81. Rocchetta HL, Burrows LL, Lam JS. Genetics of O-antigen biosynthesis in Pseudomonas aeruginosa. Microbiol Mol Biol Rev. 1999; 63(3):523–53. https://doi.org/10.1128/MMBR.63.3.523-553.1999 PMID: 10477307

82. Joiner KA. Studies on the mechanism of bacterial resistance to complement-mediated killing and on the mechanism of action of bactericidal antibody. Curr Top Microbiol Immunol. 1985; 121:99–133. https://doi.org/10.1007/978-3-642-45604-6_6 PMID: 3910367

83. Dasgupta T, de Kievit TR, Masoud H, Altman E, Richards JC, Sadovskaya I, et al. Characterization of lipopolysaccharide-deficient mutants of Pseudomonas aeruginosa derived from serotypes O3, O5, and O6. Infect Immun. 1994; 62(3):809–17. https://doi.org/10.1128/iai.62.3.809-817.1994 PMID: 8112851

84. Kadurugamuwa JL, Lam JS, Beveridge TJ. Interaction of gentamicin with the A band and B band lipopolysaccharides of Pseudomonas aeruginosa and its possible lethal effect. Antimicrob Agents Chemother. 1993; 37(4):715–21. https://doi.org/10.1128/AAC.37.4.715 PMID: 8494366

85. Wang D, Dorosky RJ, Han CS, Lo CC, Dichosa AE, Chain PS, et al. Adaptation genomics of a small-colony variant in a Pseudomonas chlororaphis 30–84 biofilm. Appl Environ Microbiol. 2015; 81 (3):890–9. https://doi.org/10.1128/AEM.02617-14 PMID: 25416762

86. Malone JG, Jaeger T, Spangler C, Ritz D, Spang A, Arrieumerlou C, et al. YfiBNR mediates cyclic di-GMP dependent small colony variant formation and persistence in Pseudomonas aeruginosa. PLoS Pathog. 2010; 6(3):e1000804. https://doi.org/10.1371/journal.ppat.1000804 PMID: 20300602

87. Pu M, Wood TK. Tyrosine phosphatase TpbA controls rugose colony formation in Pseudomonas aeruginosa by dephosphorylating diguanylate cyclase TpbB. Biochem Biophys Res Commun. 2010; 402 (2):351–5. https://doi.org/10.1016/j.bbrc.2010.10.032 PMID: 20946878

88. Remans K, Vercammen K, Bodilis J, Cornelis P. Genome-wide analysis and literature-based survey of lipoproteins in Pseudomonas aeruginosa. Microbiology (Reading). 2010; 156(Pt 9):2597–607. https://doi.org/10.1099/mic.0.040659-0 PMID: 20616104

89. Panmanee W, Gomez F, Witte D, Pancholi V, Britigan BE, Hassett DJ. The peptidoglycan-associated lipoprotein OprL helps protect a Pseudomonas aeruginosa mutant devoid of the transactivator OxyR from hydrogen peroxide-mediated killing during planktonic and biofilm culture. J Bacteriol. 2008; 190 (10):3658–69. https://doi.org/10.1128/JB.00022-08 PMID: 18310335

90. Ghazaei C. Antibiotic Resistance Profiles of Pseudomonas aeruginosa Isolates Containing Virulence Genes. Res Mol Med. 2021; 9(4):245–52.

91. Marxer M, Vollenweider V, Schmid-Hempel P. Insect antimicrobial peptides act synergistically to inhibit a trypanosome parasite. Philos Trans R Soc Lond B Biol Sci. 2016; 371(1695). https://doi.org/10.1098/rstb.2015.0302 PMID: 27160603

92. Rolff J, Schmid-Hempel P. Perspectives on the evolutionary ecology of arthropod antimicrobial peptides. Philos Trans R Soc Lond B Biol Sci. 2016; 371(1695). https://doi.org/10.1098/rstb.2015.0297 PMID: 27160599

93. Brogden KA. Antimicrobial peptides: pore formers or metabolic inhibitors in bacteria? Nat Rev Microbiol. 2005; 3(3):238–50. https://doi.org/10.1038/nrmicro1098 PMID: 15703760

94. Zanchi C, Johnston PR, Rolff J. Evolution of defence cocktails: Antimicrobial peptide combinations reduce mortality and persistent infection. Mol Ecol. 2017; 26(19):5334–43. https://doi.org/10.1111/mec.14267 PMID: 28762573

95. Srinivasan S, Waghu FH, Idicula-Thomas S, Venkatesh KV. A steady-state modeling approach for simulation of antimicrobial peptide-cell membrane interaction. Biochim Biophys Acta Biomembr. 2020; 1862(4):183242. https://doi.org/10.1016/j.bbamem.2020.183242 PMID: 32135146

96. Lazzaro BP, Zasloff M, Rolff J. Antimicrobial peptides: Application informed by evolution. Science. 2020; 368(6490). https://doi.org/10.1126/science.aau5480 PMID: 32355003

97. Gullberg E, Cao S, Berg OG, Ilback C, Sandegren L, Hughes D, et al. Selection of resistant bacteria at very low antibiotic concentrations. PLoS Pathog. 2011; 7(7):e1002158. https://doi.org/10.1371/journal.ppat.1002158 PMID: 21811410

98. Ling LL, Schneider T, Peoples AJ, Spoering AL, Engels I, Conlon BP, et al. A new antibiotic kills pathogens without detectable resistance. Nature. 2015; 517(7535):455–9. https://doi.org/10.1038/nature14098 PMID: 25561178

99. Lloyd DG, Schofield BJ, Goddard MR, Taylor EJ. De Novo Resistance to Arg(10)-Teixobactin Occurs Slowly and Is Costly. Antimicrob Agents Chemother. 2020;65(1).

100. Johnston PR, Makarova O, Rolff J. Inducible defenses stay up late: temporal patterns of immune gene expression in Tenebrio molitor. G3 (Bethesda). 2013; 4(6):947–55. https://doi.org/10.1534/g3.113.008516 PMID: 24318927

101. He J, Baldini RL, Deziel E, Saucier M, Zhang Q, Liberati NT, et al. The broad host range pathogen Pseudomonas aeruginosa strain PA14 carries two pathogenicity islands harboring plant and animal virulence genes. Proc Natl Acad Sci U S A. 2004; 101(8):2530–5. https://doi.org/10.1073/pnas.0304622101 PMID: 14983043

102. Habermann E, Neumann W. Characterization of the effective components of snake venoms. Naunyn Schmiedebergs Arch Exp Pathol Pharmakol. 1954; 223(5):388–98.

103. Fuchs PC, Barry AL, Brown SD. In vitro antimicrobial activity of MSI-78, a magainin analog. Antimicrob Agents Chemother. 1998; 42(5):1213–6. https://doi.org/10.1128/AAC.42.5.1213 PMID: 9593152

104. Andersson M, Boman A, Boman HG. Ascaris nematodes from pig and human make three antibacterial peptides: isolation of cecropin P1 and two ASABF peptides. Cell Mol Life Sci. 2003; 60(3):599–606. https://doi.org/10.1007/s000180300051 PMID: 12737319

105. Klubthawee N, Adisakwattana P, Hanpithakpong W, Somsri S, Aunpad R. A novel, rationally designed, hybrid antimicrobial peptide, inspired by cathelicidin and aurein, exhibits membrane-active

mechanisms against Pseudomonas aeruginosa. Sci Rep. 2020; 10(1):9117. https://doi.org/10.1038/s41598-020-65688-5 PMID: 32499514

106. Wick R. Porechop: adapter trimmer for Oxford Nanopore reads. 2018.

107. Wick RR, Menzel P. Filtlong. 2018.

108. Kolmogorov M, Yuan J, Lin Y, Pevzner PA. Assembly of long, error-prone reads using repeat graphs. Nat Biotechnol. 2019; 37(5):540–6. https://doi.org/10.1038/s41587-019-0072-8 PMID: 30936562

109. Nanoporetech. Medaka: Sequence correction provided by ONT research. GitHub. 2019. Available from: https://github.com/nanoporetech/medaka.

110. Wick RR, Holt KE. Polypolish: Short-read polishing of long-read bacterial genome assemblies. PLoS Comput Biol. 2022; 18(1):e1009802. https://doi.org/10.1371/journal.pcbi.1009802 PMID: 35073327

111. Hunt M, Silva ND, Otto TD, Parkhill J, Keane JA, Harris SR. Circlator: automated circularization of genome assemblies using long sequencing reads. Genome Biol. 2015; 16:294. https://doi.org/10.1186/s13059-015-0849-0 PMID: 26714481

112. Seemann T. Prokka: rapid prokaryotic genome annotation. Bioinformatics. 2014; 30(14):2068–9. https://doi.org/10.1093/bioinformatics/btu153 PMID: 24642063

113. Bolger AM, Lohse M, Usadel B. Trimmomatic: a flexible trimmer for Illumina sequence data. Bioinformatics. 2014; 30(15):2114–20. https://doi.org/10.1093/bioinformatics/btu170 PMID: 24695404

114. Seemann T. Snippy: fast bacterial variant calling from NGS reads. 2015.

115. Sochacki KA, Barns KJ, Bucki R, Weisshaar JC. Real-time attack on single Escherichia coli cells by the human antimicrobial peptide LL-37. Proc Natl Acad Sci U S A. 2011; 108(16):E77–81. https://doi.org/10.1073/pnas.1101130108 PMID: 21464330

116. Rangarajan N, Bakshi S, Weisshaar JC. Localized permeabilization of E. coli membranes by the antimicrobial peptide Cecropin A. Biochemistry. 2013; 52(38):6584–94. https://doi.org/10.1021/bi400785j PMID: 23988088

117. Team RC. R: A language and environment for statistical computing. Vienna, Austria; 2020.

118. Brooks ME, Kristensen K, Van Benthem KJ, Magnusson A, Berg CW, Nielsen A, et al. glmmTMB balances speed and flexibility among packages for zero-inflated generalized linear mixed modeling. R J. 2017; 9(2):378–400.

119. Bates D, Mächler M, Bolker B, Walker S. Fitting Linear Mixed-Effects Models Using lme4. J Stat Softw. 2015; 67(1):1–48.

120. Cumming G, Finch S. Inference by eye: confidence intervals and how to read pictures of data. Am Psychol. 2005; 60(2):170–80. https://doi.org/10.1037/0003-066X.60.2.170 PMID: 15740449

121. Cumming G. Inference by eye: reading the overlap of independent confidence intervals. Stat Med. 2009; 28(2):205–20. https://doi.org/10.1002/sim.3471 PMID: 18991332

122. Fox J. Effect Displays in R for Generalised Linear Models. J Stat Softw. 2003; 8(15):1–27.

123. Fox J, Weisberg S. An R companion to applied regression. Sage Publications; 2018.

124. Venables WN, Ripley BD. Modern applied statistics with S. 4th ed. New York: Springer; 2002.

125. Wickham H. ggplot2: Elegant graphics for data analysis. New York: Springer-Verlag; 2016.

126. Kassambara A. Ggpubr:"ggplot2" Based Publication Ready Plots. R package version 060. 2023.

127. Best DJ, Roberts DE. Algorithm AS 89: The Upper Tail Probabilities of Spearman's Rho. J R Stat Soc Ser C Appl Stat. 1975; 24(3):377–9.

128. Team SD. RStan: The R interface to Stan. R package version 2.17. 3. Available from: http://mc-stanorg. 2018.